Micromagnetic coercivity distributions and interactions in chondrules with implications for paleointensities of the early solar system

Gary Acton,[1] Qing-Zhu Yin,[1] Kenneth L. Verosub,[1] Luigi Jovane,[1,2] Alex Roth,[1] Benjamin Jacobsen,[1] and Denton S. Ebel[3]

[1] Chondrules in chondritic meteorites record the earliest stages of formation of the solar system, potentially providing information about the magnitude of early magnetic fields and early physical and chemical conditions. Using first-order reversal curves (FORCs), we map the coercivity distributions and interactions of 32 chondrules from the Allende, Karoonda, and Bjurbole meteorites. Distinctly different distributions and interactions exist for the three meteorites. The coercivity distributions are lognormal shaped, with Bjurbole distributions being bimodal or trimodal. The highest-coercivity mode in the Bjurbole chondrules is derived from tetrataenite, which interacts strongly with the lower-coercivity grains in a manner unlike that seen in terrestrial rocks. Such strong interactions have the potential to bias paleointensity estimates. Moreover, because a significant portion of the coercivity distributions for most of the chondrules is <10 mT, low-coercivity magnetic overprints are common. Therefore paleointensities based on the REM method, which rely on ratios of the natural remanent magnetization (NRM) to the saturation isothermal remanent magnetization (IRM) without magnetic cleaning, will probably be biased. The paleointensity bias is found to be about an order of magnitude for most chondrules with low-coercivity overprints. Paleointensity estimates based on a method we call REMc, which uses NRM/IRM ratios after magnetic cleaning, avoid this overprinting bias. Allende chondrules, which are the most pristine and possibly record the paleofield of the early solar system, have a mean REMc paleointensity of 10.4 μT. Karoonda and Bjurbole chondrules, which have experienced some thermal alteration, have REMc paleointensities of 4.6 and 3.2 μT, respectively.

1. Introduction

[2] The magnetic field of the early solar nebula is perhaps the most important physical parameter, after the gravitational field that governs the formation of the early solar system. Primitive meteorites, which formed 4.56 billion years ago at the beginning of the solar system, may record the physical and chemical conditions of the early solar nebula. The potential for recovering the paleomagnetic field intensity of the early solar nebula from meteorites was recognized in the founding magnetic studies conducted in the 1970s and 1980s [e.g., *Butler*, 1972; *Stacey*, 1976; *Brecher and Leung*, 1979; *Nagata*, 1979; *Sugiura et al.*, 1979; *Funaki et al.*, 1981; *Wasilewski*, 1981a] (see reviews by *Sugiura and Strangway* [1988]). Progress has been slow for nearly two decades in part because characterizing the magnetic field in the early solar nebula has proven to be a daunting task due to the unusual magnetic minerals in meteorites, to processes such as aqueous alteration, thermal metamorphism, and shock metamorphism that may have affected meteorites as they resided in their parent asteroids bodies, and to magnetic overprinting that can occur once the meteorites reach Earth [*Wasilewski and Dickinson*, 2000; *Kohout et al.*, 2004]. In the past few years, efforts to critically evaluate these complex factors have seen a resurgence [*Wasilewski et al.*, 2002; *Kletetschka et al.*, 2003, 2004, 2006; *Gattacceca and Rochette*, 2004; *Kohout et al.*, 2004].

[3] We revisit the issue of the paleomagnetism of chondrites, with special focus on chondrules in primitive meteorites. Primitive chondrites (undifferentiated and unequilibrated stony meteorites) are considered the most pristine samples, and are believed to represent the composition of the solar nebula from which they formed. They typically consist of three distinct components in varying proportions: chondrules, calcium-aluminum-rich inclusions (CAIs), and fine nebular dusts (matrices) that cement the chondrules and CAIs together. Chondrules are millimeter-

[1]Department of Geology, University of California, Davis, California, USA.
[2]Also at Istituto Nazionale di Geofisica e Vulcanologia, Rome, Italy.
[3]Department of Earth and Planetary Sciences, American Museum of Natural History, New York, New York, USA.

size spherules of rock that were formed from melting of primordial material in the accretionary disk of the solar nebula. These molten droplets cooled from above the liquidus to below the Curie temperature at a rapid rate of 10–1000 K/h [*Lofgren*, 1996], potentially locking in a thermal remanent magnetization (TRM) that records the ancient magnetic field of the solar nebula.

[4] The magnetic field of the solar nebula and the winds and jets that it produced are expected to have played an important role in the evolution of accretionary disks [e.g., *Shu et al.*, 1996, 1997; *Ferreira*, 1997; *Joung et al.*, 2004; *Donati et al.*, 2005]. One recent hypothesis, referred to as the X wind hypothesis [*Shu et al.*, 1996], predicts that magnetocentrifugally driven winds from the solar nebula pulled material from cool regions of the nebular disk to within only a few solar radii of the proto-Sun, exposing the material to heat and melting it into droplets. These droplets were then launched by the magnetic X winds out to planetary distances, and cooled rapidly en route in space. They were later aggregated into asteroids, planetesimals, and planets, where subsequently some chondrules were exposed to heating, deformation, and alteration while others remained virtually unperturbed.

[5] Whether either pristine or altered chondrules preserve a record of the magnitude of ancient magnetic fields and whether the records can be extracted is still open to much debate. Earlier studies [e.g., *Butler*, 1972] and more recent ones [e.g., *Kletetschka et al.*, 2003; *Kohout et al.*, 2004] showed that only the fusion crust or the outer 1–6 mm of the primitive meteorites are partially remagnetized as they fall through Earth's atmosphere. As a result of these findings, many studies have sought to determine if the magnetic remanence of meteorites and chondrules retains a record of the nebular magnetic field, and if so, to determine the paleofield intensity. This raises a question of how we differentiate the paleofields of meteorite parent bodies from that of the early solar nebula. Notably, *Sugiura et al* [1979] showed that the chondrules in chondrites pass a classical paleomagnetic conglomerate test. In this version of the test, the chondrules from a meteorite have natural remanent magnetization (NRM) directions that are relatively stable but randomly oriented with respect to each other, indicating that they acquired their NRMs prior to accretion into the meteorite parent body. This has since been verified in studies by *Funaki et al.* [1981], *Collinson* [1987], *Morden and Collinson* [1992], and *Wasilewski et al.* [2002]. It follows that absolute paleointensity determinations on at least some chondrules have the potential to provide information about the strength of magnetic fields present at the inception of the solar system.

[6] Determining the paleointensity of rocks is difficult, even for terrestrial rocks. For example, the most reliable experimental methods, such as the various forms of the Thellier-Thellier paleointensity experiments, require that a sample be heated repeatedly to peak temperatures of 500°C to 700°C. When subjected to these temperatures, most rocks alter to varying extents or their magnetic minerals undergo phase transformations. Furthermore, only a small percentage of terrestrial rocks contain dispersed single-domain (SD) or small pseudosingle-domain (PSD) magnetic grains (e.g., basaltic glass) that are the most appropriate for paleointensity determinations [e.g., *Selkin and Tauxe*,

2000; *Valet*, 2003; *Dunlop et al.*, 2005]. As a result, the success rate is quite low even when samples are carefully selected to have the most desirable magnetic properties. These problems are exacerbated in meteorite studies because the material itself is rare and the primary magnetic minerals, such as Fe-Ni alloys (kamacite, taenite, and tetrataenite), iron sulfides, and magnetite, are very likely to be oxidized or to undergo phase transitions when heated. Such alteration was evident in the first attempts to conduct Thellier-Thellier experiments on meteorites, in which *Banerjee and Hargraves* [1972] and *Butler* [1972] noted a change in the NRM versus TRM slopes at temperatures as low as 150°C for sample of the Allende meteorite. Subsequently, *Wasilewski* [1981a] found that multiple irreversible transitions occurred at temperatures as low as 50°C for the matrix of the Allende meteorite.

[7] In order to overcome this problem, recent paleofield studies of meteorites have relied on paleointensity proxies such as the ratio of the NRM to saturation isothermal remanent magnetization (IRM), with all measurements done at room temperature [e.g., *Wasilewski and Dickinson*, 2000; *Kletetschka et al.*, 2003; *Gattacceca and Rochette*, 2004]. Usually, neither the NRM nor the saturation IRM are subjected to demagnetization, in which case the ratio is referred to as REM. Alternatively, the NRM and IRM can be demagnetized in a low alternating field (AF), such as 20 mT [*Cisowski and Fuller*, 1986; *Wasilewski et al.*, 2002; *Antretter and Fuller*, 2002; *Kletetschka et al.*, 2005]. The goal here is to remove low-coercivity overprints and retain only that part of the coercivity spectrum representative of the characteristic remanent magnetization (ChRM). High-coercivity overprints are also possible but generally are much rarer than low-coercivity overprints. We refer to this ratio as the REMc (where the "c" is for the coercivity of the ChRM). Most recently, the ratio of change of the NRM to the change of IRM over a discrete range of AF demagnetization levels, designated the REM′, has been used as an alternate means of dealing with secondary magnetization components [*Gattacceca and Rochette*, 2004].

[8] Experimental calibration suggests that the paleofield in μT is ~3000 times the REM, REMc, or REM′ values [*Kletetschka et al.*, 2004; *Gattacceca and Rochette*, 2004] (see Figure 1 from either *Kletetschka et al.* [2004] or *Gattacceca and Rochette* [2004]). It is reported that the conversion factor applies over a range of paleofields from ~1 to 1000 μT, has an uncertainty of about a factor of two, and is applicable to magnetite, titanomagnetites, FeNi alloys, and pseudosingle-domain (PSD) size pyrrhotite [*Gattacceca and Rochette*, 2004]. Recently, *Yu* [2006] showed that the NRM/IRM ratios are sensitive to magnetic grain size, magnetic mineralogy, and, to a lesser degree, magnetic anisotropy. He also found a conversion factor half that quoted above from a single historic volcanic flow with a well-constrained paleointensity determination. Hence there is still much to learn about the accuracy of the conversion factor, the conditions under which the method is applicable, and the precision of the resulting paleofield estimates.

[9] As noted in most studies that have used the REM method, erroneous paleofield estimates result if the NRM contains secondary magnetization components (overprints) in addition to the ChRM (where the ChRM is presumed to

be the NRM component acquired by chondrules early in the formation of the solar system, e.g., prior to amalgamation into a meteorite). The secondary components would be expected to be rather common because meteorites may be partially remagnetized by prior impacts or by association with planetesimals, may be subjected to large magnetic fields from lightning strikes or by hand magnets used by experimenters, or may acquire a strong viscous remanent magnetization (VRM) while sitting in the geomagnetic field [*Wasilewski and Dickinson*, 2000; *Antretter and Fuller*, 2002; *Kletetschka et al.*, 2003; *Kohout et al.*, 2004]. Generally, these overprints affect the lower part of the magnetic coercivity spectrum. Hence REMc and REM′ values may provide valid paleofield estimates since they avoid using the low-coercivity portion of the spectrum.

[10] In order to better understand the coercivity distributions in meteorites and the ways that the variations in coercivity affect the paleointensity estimates, we have conducted paleomagnetic and rock magnetic investigations on chondrules from three meteorites. In this paper, we specifically focus on characterizing the microcoercivities and the interactions of magnetic grains in chondrules and on relating these properties to the AF demagnetization behavior of the NRM and IRM and to estimates of paleointensity based on REM, REMc, and REM′. Using first-order reversal curves (FORCs) [*Pike et al.*, 1999, 2001b], we map magnetic interactions between magnetic grains that are quite unlike those seen in terrestrial rocks. These interactions highlight possible difficulties in obtaining paleointensity estimates from some meteorites.

2. Background

2.1. Samples

[11] We analyzed 32 chondrules from the Allende, Karoonda, and Bjurbole meteorites. The diameters of the chondrules range from ∼0.1 mm to over 1 mm, with masses varying from 1 to 75 mg. Of the 32 chondrules, 11 are from the Allende meteorite, 11 are from Bjurbole, and 10 are from Karoonda (Table 1). None of the chondrules include fusion crusts or are from the outer few mm of the meteorites.

[12] The Allende meteorite is from an observed meteorite fall that occurred in February 1969 over the Allende River Valley in Mexico. It is a class CV3 meteorite (C for carbonaceous, V for the type meteorite Vigarano for this group, and 3 for the metamorphic grade, where 3 is the lowest thermal metamorphic grade and 6 is the highest grade and grades 2 and 1 refer to increasing degrees of aqueous alteration). The Karoonda meteorite is a CK4 carbonaceous chondrite (K for Karoonda type) from a fall in 1930 in South Australia. The Bjurbole meteorite is an L/LL4 ordinary chondrite (L for low iron and LL for very low iron and low metal) from a fall that occurred in March 1899 in Finland.

[13] The chondrules analyzed were samples of opportunity that were originally collected for tomographic and geochemical analyses. Tomographic scans were obtained for 24 of 32 the chondrules (all except samples Bjurbole-L01 to L08) prior to the magnetic measurements [*Ebel et al.*, 2007]. The scans involved subjecting each chondrule to

∼10 mW of X-ray power, without heating or exposure to large magnetic fields.

2.2. Previous Magnetic Studies

[14] Previous paleomagnetic and rock magnetic investigations have been conducted on all three meteorites in this study. The magnetic properties of Allende meteorite were studied by *Banerjee and Hargraves* [1972], *Butler* [1972], *Brecher and Arrhenius* [1974], *Herndon et al.* [1976], *Brecher* [1977], *Lanoix et al.* [1977], *Lanoix and Strangway* [1978], *Nagata* [1979], *Sugiura et al.* [1979], *Wasilewski* [1981a], *Sugiura and Strangway* [1985], *Wasilewski and Dickinson* [2000], and *Thorpe et al.* [2002]. The primary magnetic minerals were identified as Ni-rich NiFe alloys (mainly taenite), iron sulfide, and magnetite [*Banerjee and Hargraves*, 1972; *Butler*, 1972; *Wasilewski*, 1981a]. The Curie temperature was 550–620°C, and most of the magnetization unblocked around 320°C [*Butler*, 1972; *Sugiura et al.*, 1979; *Wasilewski*, 1981a]. Median destructive fields (MDFs) for chondrules ranged from 15 to 80 mT, whereas the bulk meteorite and matrix had MDFs of 90 mT and >100 mT, respectively [*Sugiura et al.*, 1979; *Wasilewski*, 1981a]. Thermomagnetic analyses indicated transitions at 50–75°C, 125–150°C, and 320°C, with irreversible heating and cooling curves [*Banerjee and Hargraves*, 1972; *Butler*, 1972; *Wasilewski*, 1981a]. The Verwey transition characteristic of magnetite at ∼110–130 K was not observed [*Wasilewski*, 1981a]. *Sugiura et al.* [1979] reported a positive conglomerate test using oriented chondrules, indicating that the chondrules had acquired their ChRM directions prior to being incorporated into the meteorite. Thellier-Thellier paleofield estimates of 110 μT were obtained on bulk meteorite samples by *Banerjee and Hargraves* [1972] and *Butler* [1972], using only the low-temperature NRM and partial TRM component, whereas *Lanoix et al.* [1977] and *Lanoix and Strangway* [1978] obtained estimates of 100–700 μT using higher-temperature components. In contrast, *Wasilewski* [1981a] found REM values for the Allende chondrules ranging from 0.0004 to 0.005, which correspond to paleofield estimates of 1.2 to 15 μT.

[15] The magnetic properties of the Bjurbole meteorite have been studied by *Brecher and Ranganayaki* [1975], *Wasilewski* [1988], *Wasilewski and Dickinson* [2000], *Wasilewski et al.* [2002], *Rochette et al.* [2003], and others. The primary magnetic minerals were identified as tetrataenite, kamacite, taenite, and plessite [*Wasilewski*, 1988]. Thermomagnetic curves show transitions at 550°C (tetrataenite) and 650°C (kamacite), with irreversible conversion of tetrataenite to taenite upon cooling from temperatures above 550°C [*Wasilewski*, 1988]. *Wasilewski et al.* [2002] identified an ultrasoft coercivity component in Bjurbole chondrules that acquired a significant magnetization when the chondrules were cooled to 78 K and then reheated to 300 K in the presence of a magnetic field (<50 μT). They also showed that the NRM directions from 83 oriented subsamples were random, arguing for a preaccretion NRM. A compilation of REM values from Bjurbole chondrules shows large variations, with 14% > 0.1 and 10% < 0.001 [*Wasilewski and Dickinson*, 2000].

[16] Magnetic studies for the Karoonda meteorite consist mainly of a Thellier-Thellier paleofield estimate on the

Table 1. Magnetic Properties and Paleointensity Proxies[a]

Sample	Magnetic Properties									Paleointensity Proxies					ChRM Interval, mT
	Mass, g	Susceptibility, 10^{-8} m^3/kg	M_r, A m^2/kg	M_s, A m^2/kg	B_{cr}, mT	B_c, mT	M_r/M_s	B_{cr}/B_c	Slope Correction, A m^2/mT	REM $\times$ 3000	REMc $\times$ 3000	REMc SD $\times$ 3000	REM' $\times$ 3000	REM' SD $\times$ 3000	
Allende4284-chA	0.075	61	0.0058	0.0574	47.83	10.39	0.102	4.603	−1.13E-08	14.96	15.94	2.28	31.16	225.05	20–50
Allende4293-chA	0.030	325	0.0465	0.5130	34.98	11.71	0.091	2.987	−4.08E-09	11.59	6.30	2.12	0.51	13.55	10–45
Allende4308-chA	0.035	5483	0.2800	6.8771	24.75	5.75	0.041	4.304	−2.24E-08	12.74	11.09	4.49	3.93	24.50	10–45
Allende4327-ch1	0.043	77	0.0087	0.0830	86.42	11.64	0.105	7.424	−1.43E-08	156.69	16.07	1.92	12.12	99.74	18–50
Allende4327-ch2	0.007	91	0.0187	0.1526	107.80	20.91	0.123	5.155	−1.08E-09	51.78	5.89	0.86	2.70	86.16	20–50
Allende4327-ch3	0.022	68	0.0104	0.1140	81.97	14.03	0.091	5.842	−4.95E-09	14.94	13.15	0.91	6.21	19.01	25–50
Allende4327-ch4	0.004	240	0.0160	0.3293	53.39	7.60	0.049	7.021	−5.83E-10	40.12	36.22	11.75	76.51	73.03	14–50
Allende4327-ch5	0.023	57	0.0148	0.1051	97.39	22.51	0.140	4.327	−3.84E-09	10.57	16.43	2.19	16.39	79.67	20–50
Allende4327-ch6	0.010	350	0.0678	0.5994	45.74	15.85	0.113	2.886	−1.96E-09	56.58	9.07	2.18	9.69	15.49	20–50
Allende4327-ch8	0.016	628	0.1032	1.0194	35.26	11.74	0.101	3.003	−2.46E-09	61.19	8.63	3.64	24.86	20.51	12–30
Allende4448-ch1	0.039	261	0.0614	0.3521	32.79	14.49	0.175	2.263	−8.65E-09	178.27	16.15	7.64	40.87	93.38	20–50
Bjurbole-2	0.002	650	0.0950	2.3065	351.50	15.61	0.041	22.518	−1.22E-08	ND	ND	ND	ND	ND	ND
Bjurbole-4	0.010	224	0.0521	0.5676	224.30	23.38	0.092	9.594	−5.38E-09	ND	ND	ND	ND	ND	ND
Bjurbole-7	0.017	249	0.0127	0.7865	251.60	6.72	0.016	37.418	−5.39E-09	2.95	1.43	0.14	0.62	9.33	12–35
Bj-L01	0.016	2444	0.7906	6.2563	368.60	13.20	0.126	27.924	−1.93E-08	27.49	4.91	1.17	b	126.07	10–60
Bj-L02	0.019	213	0.1756	0.8805	451.00	56.76	0.199	7.946	−1.24E-08	5.95	6.96	0.87	0.24	32.14	10–60
Bj-L03	0.020	828	0.3233	2.1970	441.00	46.72	0.147	9.439	−6.80E-09	11.23	9.27	0.34	20.06	46.73	12–25
Bj-L04	0.013	88	0.1179	0.4177	312.10	71.02	0.282	4.395	−7.99E-09	7.69	9.11	0.22	12.35	13.15	50–70
Bj-L05	0.003	67	0.0809	0.2633	354.40	114.80	0.307	3.087	−1.12E-09	11.40	13.39	2.83	b	66.27	10–60
Bj-L06	0.019	218	0.0861	0.5042	218.00	48.61	0.171	4.485	−5.54E-09	1.52	6.20	1.54	b	21.01	40–80
Bj-L07	0.008	1025	0.6099	4.6013	407.00	40.49	0.133	10.052	−2.25E-08	1.65	0.67	0.17	b	9.87	40–80
Bj-L08	0.032	41	0.0007	0.0068	812.50	26.75	0.105	30.374	−1.18E-08	32.03	16.29	5.30	55.43	224.54	10–60
Karoonda-10	0.014	5221	0.8543	7.6857	23.08	9.48	0.111	2.435	−9.13E-09	91.82	23.82	9.15	46.98	26.49	12–35
Karoonda-13	0.008	2288	0.4005	3.6063	26.73	10.76	0.111	2.484	−4.00E-09	55.43	4.56	1.55	6.69	12.15	12–35
Karoonda-14	0.009	6122	1.4456	9.8911	27.02	12.96	0.146	2.085	−6.31E-09	33.61	3.35	1.64	6.44	9.70	12–35
Karoonda-15	0.006	3593	0.7853	5.4667	27.81	12.16	0.144	2.287	−3.08E-09	42.82	2.68	1.01	3.61	7.23	12–35
Karoonda-16	0.010	5650	1.0260	8.3510	23.03	10.17	0.123	2.265	−6.21E-09	66.45	4.66	0.97	3.80	7.35	12–35
Karoonda-18	0.009	2544	0.5506	3.7489	29.35	12.90	0.147	2.275	−3.69E-09	43.71	5.86	2.03	13.01	9.35	12–25
Karoonda-22	0.004	4110	0.9850	6.8000	26.65	12.35	0.145	2.158	−2.77E-09	64.84	6.63	2.63	14.09	14.66	12–35
Karoonda-23	0.008	2470	0.6324	3.9613	27.97	13.01	0.160	2.150	−3.53E-09	77.39	9.62	4.15	20.60	15.68	12–35
Karoonda-25	0.004	3490	0.6770	5.4375	26.38	10.79	0.125	2.445	−1.87E-09	103.41	18.73	6.90	22.99	44.23	18–50
Karoonda-30	0.001	1360	0.3128	2.1330	36.51	14.94	0.147	2.444	−1.88E-10	42.18	9.93	2.22	8.43	16.35	18–35

[a]M_r, saturation remanent magnetization; M_s, saturation magnetization; B_{cr}, coercivity of remanence; B_c, coercivity; slope correction, the high-field (paramagnetic) slope correction estimated from the hysteresis loop; REM, REMc, and REM' and the standard deviations (SD) are defined in the text. We have multiplied these values by 3000 to convert them to paleointensity proxies with units of microteslas. ChRM interval, the demagnetization interval over which the characteristic remanent magnetization is resolved. This interval is used in calculating REMc and REM' values. Read −1.13E-08 as −1.13 × 10⁻⁸. ND, not determined.

[b]Negative values caused by the lack of decay of the NRM in conjunction with instrument noise.

bulk meteorite, which resulted in a paleointensity estimate of 89 μT [*Nagata*, 1979].

3. Methods

[17] Only nondestructive techniques were used in this study in order to allow subsequent investigations to be conducted on the chondrules. In total, we measured (1) the NRM, (2) the anhysteretic remanent magnetization (ARM), imparted in a 100 mT AF field with a 50 μT biasing field, (3) the IRM, imparted with a impulse magnetic field of 1 T, (4) hysteresis properties, (5) coercivities of remanence, (6) IRM acquisition curves, (7) first-order reversal curve (FORC) distributions, and (8) magnetic susceptibility.

[18] All measurements were made in the Paleomagnetism Laboratory at the University of California, Davis. The NRM, ARM, and IRM were measured following progressive AF demagnetization up to 80 mT, with steps every 2 mT up to 20 mT and steps every 5 mT thereafter. The measurements were made with a long-core cryogenic magnetometer (2G Enterprises Model 755-1.65UC) with an automated track and in-line AF, ARM, and IRM units. Hysteresis properties, coercivities of remanence, and FORC distributions were measured with an alternating gradient magnetometer (AGM) (Princeton Measurement Corporation model MicroMag 2900 AGM). IRM acquisition experiments were conducted using both the cryogenic and AGM magnetometers. Susceptibilities were measured with a KappaBridge (AGICO model KLY 2).

[19] For the NRM, ARM, and IRM measurements, the samples were glued to the ends of ~1-cm-long pieces of wooden or plastic sticks or placed between small pieces of transparent tape, which allowed us to handle them more easily and maintain their relative orientation. Given the relatively small magnetic moments, we were careful to magnetically clean the magnetometer tray on which the samples were placed, especially following ARM and IRM acquisitions. In addition, we included blanks in all measurement runs to monitor the noise level, which is ~5×10^{-10} A m^2 for the cryogenic magnetometer.

[20] Because the NRM for many of the chondrules decreased to the noise level of the magnetometer following demagnetization to 50–60 mT, we made 3 to 6 repeat measurements at demagnetization levels of 20 mT and higher for some samples to improve the signal-to-noise ratio and to assess the quality of the results. For each repeat measurement, we also repeated the three-axis AF demagnetization, randomly alternating which axis was demagnetized first, second, and third, with the aim of reducing ARMs acquired during AF demagnetization. Meteorites are notorious for their erratic AF demagnetization behavior in which the magnetization increases and decreases in a "zigzag" pattern rather than decaying with progressive demagnetization [e.g., *Morden*, 1992]. This behavior was attributed by *Morden* [1992] to a large percentage of magnetic grains with very low coercivity, which result in an ultrasoft component of magnetization. Magnetic grains with such low coercivities rapidly acquire new magnetizations in ambient fields as a VRM or during AF demagnetization in high fields as an ARM.

[21] For hysteresis and FORC measurements, the samples were removed from the sticks or tape and mounted on the

tip of an AGM phenolic probe with vacuum grease. The FORC distributions, which provide information about the microcoercivity and magnetic interactions [e.g., *Pike et al.*, 1999, 2001a; *Roberts et al.*, 2000; *Muxworthy and Dunlop*, 2002], were generally obtained from 60 to 120 FORCs for each sample using a saturating field of 1 or 1.3 T. FORC diagrams were created with FORCIT software, which is available at http://paleomag.ucdavis.edu/software.html.

[22] Calculation of the three paleointensity proxies, REM, REMc, and REM′, is straightforward since all of these proxies are ratios of the NRM to the IRM, although they are taken over different portions of the coercivity spectrum. Only one possible value exists for the REM, whereas REMc and REM′ can be computed over many different parts of the coercivity spectrum. For any of the REMc and REM′ values to be relevant as paleointensity proxies, they should be computed for the part of the coercivity spectrum that is representative of the primary magnetization, which generally is assumed to be the ChRM. As an example, let us consider the NRM and IRM of a chondrule that was measured after AF demagnetization at 0, 10, 20, 40, and 80 mT and for which the ChRM can be resolved for all demagnetization steps above 20 mT. We use the nomenclature NRM20 and IRM20 to represent the NRM and IRM after 20 mT AF demagnetization, respectively. In that case, the REM = NRM0/IRM0 and the REMc can be calculated from NRM20/IRM20, NRM40/IRM40, or NRM80/IRM80. For a well-resolved ChRM, the REMc values should all be equivalent. REM′ can be calculated as any of the REMc values or, as originally advocated by *Gattacceca and Rochette* [2004], it could be calculated for a range of coercivities, i.e., REM′ = (NRM20−NRM40)/(IRM20−IRM40), (NRM20−NRM80)/(IRM20−IRM80), or (NRM40−NRM80)/(IRM40−IRM80). For samples that have no secondary overprints and that have NRMs and IRMs that decay progressively over the entire range of AF demagnetization fields used, the REM, REM′ and REMc values should be the same.

[23] Data acquired in this study are archived in the MagIC database (http://earthref.org) or in the FORCopedia database (http://forc.ucdavis.edu/forcopedia.html), including tables with magnetic remanence measurements at all demagnetization steps, hysteresis and FORC measurements as well as additional orthogonal vector diagrams, IRM versus NRM plots, hysteresis loop plots, and FORC diagrams.

4. Results
4.1. Natural Remanent Magnetization

[24] Prior to demagnetization, the NRMs of the chondrules ranged from 2.8×10^{-5} to 3.4×10^{-3} A m^2/kg for Allende, 7.4×10^{-6} to 4.5×10^{-3} A m^2/kg for Bjurbole, and 6.2×10^{-3} to 2.4×10^{-2} A m^2/kg for Karoonda. Median NRMs prior to demagnetization were 2.2×10^{-4}, 2.6×10^{-4}, and 1.4×10^{-2} A m^2/kg for Allende, Bjurbole, and Karoonda, respectively (Figure 1).

[25] AF demagnetization of the NRM illustrates that most samples have a low-coercivity component that can be removed in alternating fields of 4 to 20 mT (Figure 2). Generally, AF demagnetization at 20 mT removed 65%, 34%, and 96% of the NRM of Allende, Bjurbole, and Karoonda, respectively. Median destructive fields (MDFs)
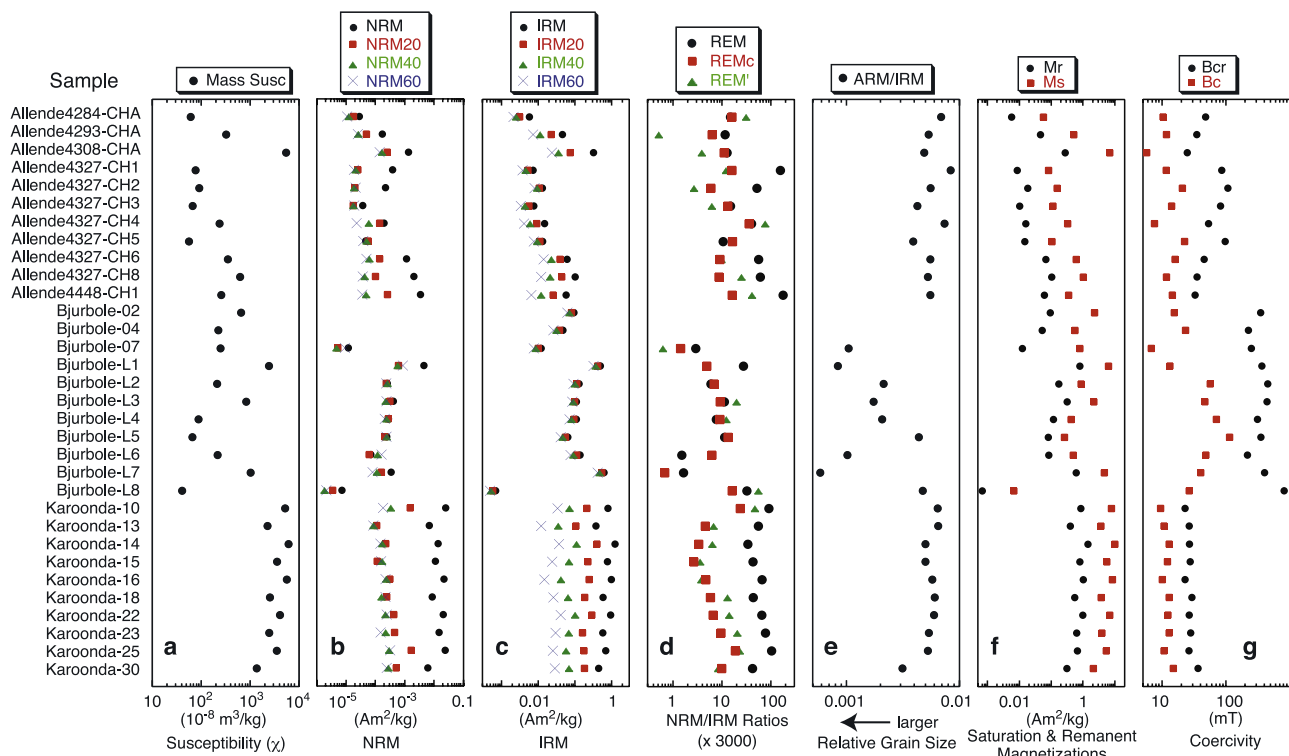
Figure 1. Rock magnetic properties of the 32 chondrules analyzed in this study: (a) Mass susceptibility; (b) NRM, NRM20 (i.e., the NRM after 20 mT AF demagnetization), NRM40, and NRM60; (c) IRM, IRM20, IRM40, and IRM60; (d) paleointensity proxies REM, REM′, and REMc; (e) magnetic grain size proxy, ARM/IRM; (f) saturation remanent magnetization (M_r) and saturation magnetization (M_s); and (g) coercivity of remanence (B_{cr}) and coercivity (B_c).

for the NRMs are thus less than 20 mT for most of the Allende and all of Karoonda samples as well as for four of the Bjurbole samples. The low MDFs for the NRMs may be more indicative of recently acquired overprints rather than a primary magnetization. Indeed, entry into Earth's atmosphere, heating to ambient Earth temperature in the presence of the geomagnetic field, collection and storage of samples, and tomographic imaging may all have contributed to some low-coercivity overprinting.

[26] After removal of the low-coercivity component, higher levels of AF demagnetization resulted in moderate to negligible decay of the remaining NRM. In the cases where little or no further reduction of the NRM occurred, the paleomagnetic directions were relatively stable and well resolved, giving "stable endpoints" on orthogonal vector component demagnetization diagrams. This was most typical of the Allende and Bjurbole samples. The Allende samples displayed more directional variability above 50 mT mainly owing to noise (Figure 3). In the cases where further decay of the NRM occurred after removing the low-coercivity component, the demagnetization paths were relatively linear and decayed to a stable endpoint. This was most typical of the Karoonda samples (Figure 2).

4.2. Anhysteretic Remanent Magnetization

[27] The ARM acquired by the samples was within an order of magnitude of the NRM. Curiously, the ARM before demagnetization was typically smaller than the original NRM. In addition, the MDFs for the ARM were more than a factor of two higher than for the NRM

(Figures 1 and 3). Both of these observations indicate that the mechanism by which the NRM was acquired is not well replicated by the ARM. Basically, the ARM is distributed much more evenly across the 0–100 mT coercivity spectrum than the NRM. The NRM is much more strongly concentrated in the very low-coercivity range (0 to 20 mT) and has a high-coercivity component that extends beyond 100 mT. Bjurbole is an exception, as the ARM acquired is small to negligible relative to the NRM that remained in the samples following AF demagnetization (Figure 2). As with the NRM, the ARM displays some erratic AF demagnetization behavior, particularly above about 50 or 60 mT (Figures 2 and 3).

4.3. Isothermal Remanent Magnetization

[28] The IRM acquired by the samples was generally about 1 to 2 orders of magnitude greater than the initial NRM (Figure 1). On average, AF demagnetization up to 20 mT removed 40%, 14%, and 70% of the IRM for Allende, Bjurbole, and Karoonda, respectively. Even AF demagnetization up to 80 mT only removed 40% of the IRM for the Bjurbole chondrules, whereas it removed 76% and 98% of the IRM for Allende and Karoonda samples (Figures 2 and 3). MDFs are thus higher for the IRM than for the ARM or NRM.

[29] The IRM decayed steadily with progressive AF demagnetization and gave linear demagnetization paths in orthogonal plots for all but two chondrules: Allende4284-CHA and Allende4308-CHA acquired a small but significant IRM component perpendicular to the direction in
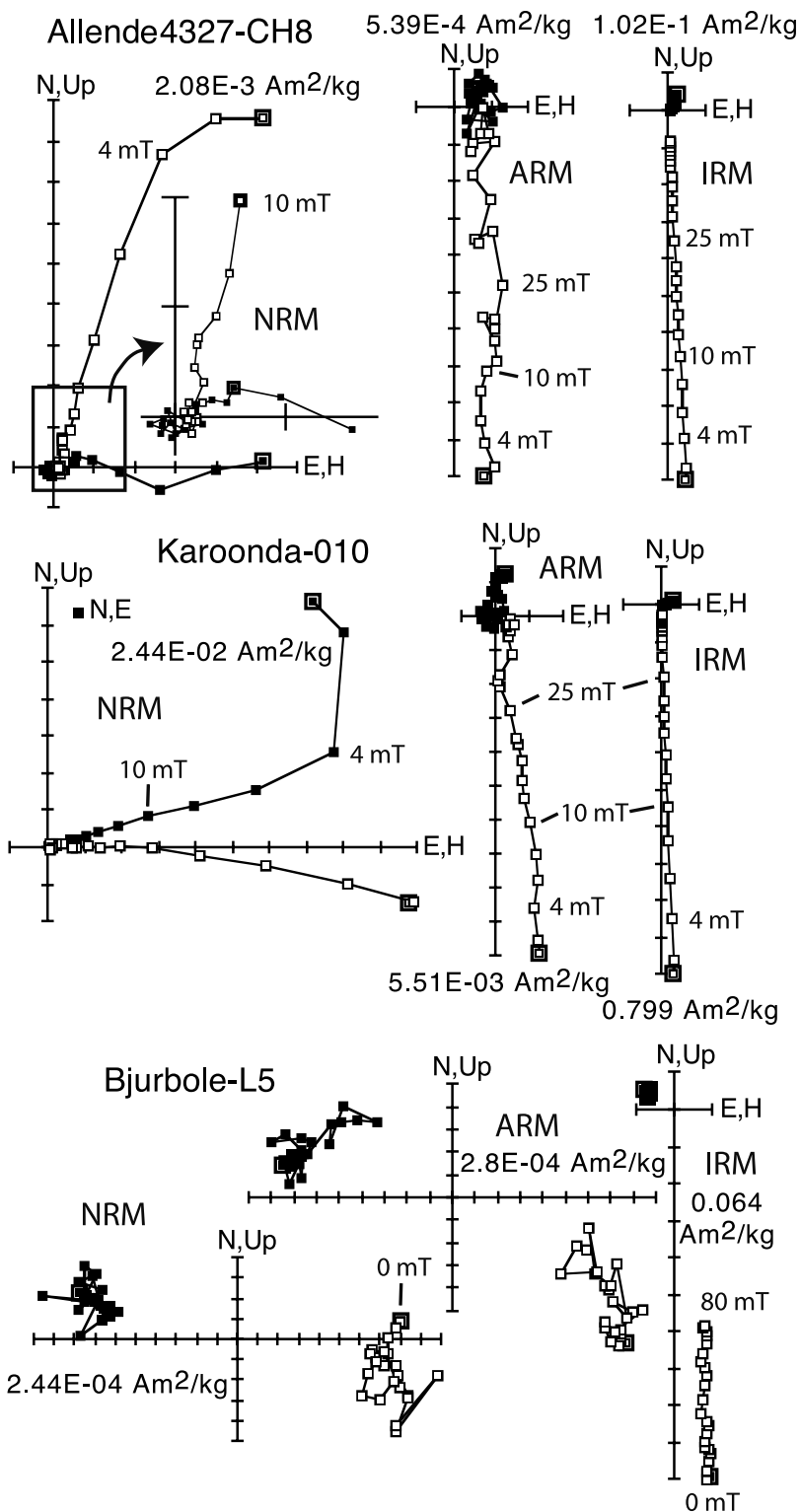
Figure 2. Representative orthogonal demagnetization plots for the NRM, ARM, and IRM of (top) an Allende chondrule, (middle) a Karoonda chondrule, and (bottom) a Bjurbole chondrule. Solid symbols are in the horizontal plane, and open symbols are in a vertical plane.

which the IRM was imparted. Repeat IRM acquisition and demagnetization experiments indicate that this is a property of these two samples, which may be caused by anisotropy of large magnetic grains.

4.4. IRM Acquisition

[30] Like the AF demagnetization of the IRM, IRM acquisition gives an indication of the distribution of the coercivity of remanence. Most AF demagnetizers are lim-
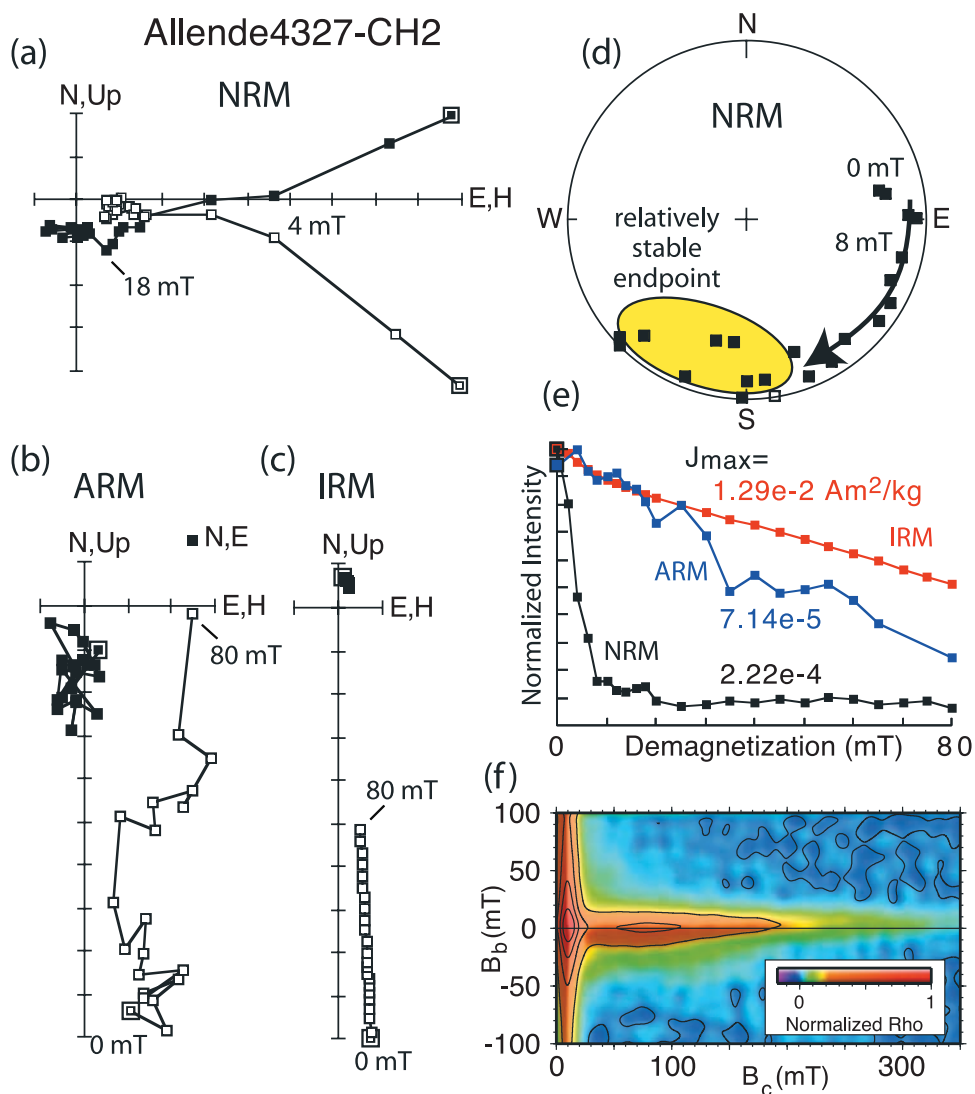
Figure 3. Representative orthogonal demagnetization plots for the (a) NRM, (b) ARM, and (c) IRM of an Allende chondrule; (d) the NRM directions plotted on a stereographic projection, which illustrates the progressive removal of a lower-coercivity overprint; (e) the decay of the normalized NRM, ARM, and IRM and (f) the FORC distribution. The decay of the IRM illustrates that about 50% of the remanent coercivity is above 80 mT, and the FORC distribution indicates that the coercivity distribution extends beyond 300 mT with little magnetic interaction for grains with coercivities above about 10 mT.

ited to fields of ∼100 mT, whereas IRM acquisition provides data up to ∼1 T and thus can be used to resolve the higher part of the coercivity distribution.

[31] Allende chondrules reached 50% of magnetic saturation in fields <100 mT, 95% of saturation in fields <300 mT, and the remanence continued to increase very slightly up to about 600 mT (Figure 4). Karoonda samples reached 50% of saturation in fields <30 mT, 95% of saturation in fields <130 mT, and were fully saturated by about 200 mT. In contrast, the IRM acquisition curves for the Bjurbole samples did not completely flatten with increasing field all the way out to 1 or 1.3 T, and the samples never reached saturation, although they did appear to be approaching saturation at 1.3 T. They generally reached 50% of the maximum IRM by 300 to 500 mT.

[32] The remanent coercivity distributions for the Allende and Karoonda chondrules are shaped like unimodal

Gamma, Poisson, or logarithmic Gaussian (lognormal) distributions (Figure 5). Similarly shaped distributions occur in terrestrial rocks and have been modeled using lognormal distributions by *Egli* [2004]. The distributions for Bjurbole chondrules are bimodal or trimodal (Figures 5 and 6). The lowest-coercivity component has a peak <20 mT and its amplitude is typically several times larger than the intermediate component and an order of magnitude larger than the high-coercivity component. This lowest mode is best resolved by the cryogenic magnetometer using data from AF demagnetization of the saturation IRM (Figure 6). The intermediate-coercivity component has a peak around 100 mT and is typically several times larger than the high-coercivity component. Most commonly, the low- and intermediate-coercivity modes coalesce into a single mode with a peak between 10 and 100 mT. The highest-coercivity component has a broad peak that lies between 400 to
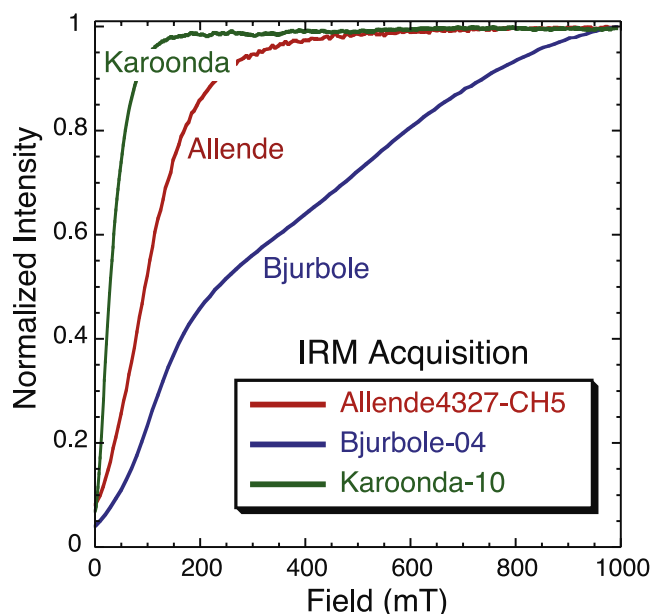
Figure 4. Representative IRM acquisition curves for Allende, Karoonda, and Bjurbole chondrules.

700 mT. This component falls off near 1.3 T but the shape of the distribution is not fully resolved because its upper limit exceeds the maximum applied field.

4.5. Hysteresis Loops and Remanence Curves

[33] Hysteresis loops along with backfield remanence curves can be used to determine the saturation magnetization (M_s), saturation remanent magnetization (M_{rs}), bulk coercivity (B_c), and bulk coercivity of remanence (B_{cr}). Because coercivities are given in SI units of millitesla (mT), we follow the nomenclature advocated by *Shive* [1986], in which B_c and B_{cr} are used rather than H_c and H_{cr}. The ratios M_{rs}/M_s and B_{cr}/B_c have been used as proxies for grain size, where smaller M_{rs}/M_s and larger B_{cr}/B_c values indicate larger grain sizes [*Wasilewski*, 1973; *Day et al.*, 1977]. Grain size fields (single-domain (SD), pseudosingle-domain (PSD), and multidomain (MD)) have been defined for Day plots [*Day et al.*, 1977], in which B_{cr}/B_c values are plotted versus M_{rs}/M_s values. Although developed for magnetite, the grain size fields are commonly taken as indicators of relative grain sizes for other magnetic minerals.

[34] Hysteresis loops for Allende and Karoonda chondrules are sigmoidal shaped with differences mainly in squareness (M_{rs}/M_s) and high-field slope (Figure 7a). The Bjurbole chondrules have loops that barely close at 1 T because of the presence of the high-coercivity component. Several of the loops are "wasp-waisted" (e.g., sample Bjurbole-L01), with the loop narrowing at low applied fields and then widening at higher applied fields (Figure 7b). This is indicative of the existence of at least two distinct coercivity distributions, one with low and one with high coercivity [e.g., *Wasilewski*, 1973]. Other Bjurbole hysteresis loops are relatively narrow over all applied fields (−1 to 1 T) and have bulk coercivities <25 mT, with the bulk coercivity of Bjurbole-7 being only 6.7 mT. High-field slopes are low for all the Karoonda chondrules and variable for the Allende chondrules.

Determination of a high-field slope in the Bjurbole chondrules is hampered by their high-coercivity component.

[35] The most notable features in the magnetic properties from hysteresis measurements are (1) relatively high B_{cr} values (>200 mT), variable B_c values (6 < B_c < 115 mT), and generally high B_{cr}/B_c ratios of the Bjurbole chondrules, (2) nearly uniform magnetic properties of the Karoonda chondrules, (3) the relatively high susceptibility and magnetization of Allende4308-CHA, and (4) the relatively low susceptibility and magnetization of Bjurbole-L08 (Figures 1 and 8). The Bjurbole chondrules plot mainly from the lower middle to the lower right side of a Day plot (Figure 8), showing similarities to L6 chondrites and falling in the MD grain size field. The exceptions are Bjurbole-L04, -L05, and −L06 chondrules, which have intermediate M_{rs}/M_s ratios and plot in the PSD field or just to the right of it. The similarity of the Bjurbole chondrules to L6 chondrites is most likely due to the presence of tetrataenite in them. The Allende chondrules straddle the PSD/MD boundary whereas the Karoonda chondrules cluster tightly in the lower portion of the PSD field.

4.6. FORC Distributions

[36] A magnetic grain magnetized in one direction will flip to the opposite direction when the direction of the magnetic field is inverted and increased to the switching field, which, for a single grain, is equivalent to the coercivity of the grain. The small rock pieces used in micromagnetic analyses typically have very large numbers of grains (hundreds to many billions) that have different coercivities and that can have their intrinsic coercivities modified by neighboring grains. The coercivity distributions and the interactions between the grains can be mapped using FORC diagrams, which are created by probing the interior of a hysteresis loop with multiple FORCs [e.g., *Pike et al.*, 1999, 2001a; *Roberts et al.*, 2000; *Muxworthy and Dunlop*, 2002]. Because the measurements are made in the
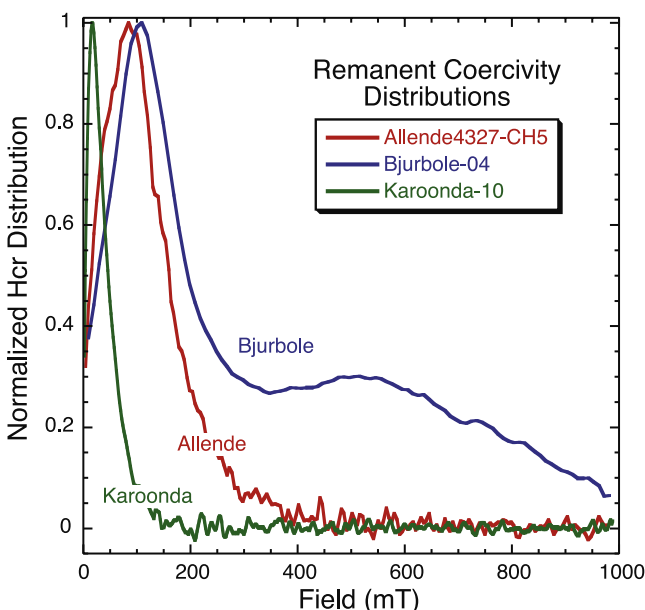

Figure 5. Representative remanent coercivity distributions for Allende, Karoonda, and Bjurbole chondrules.
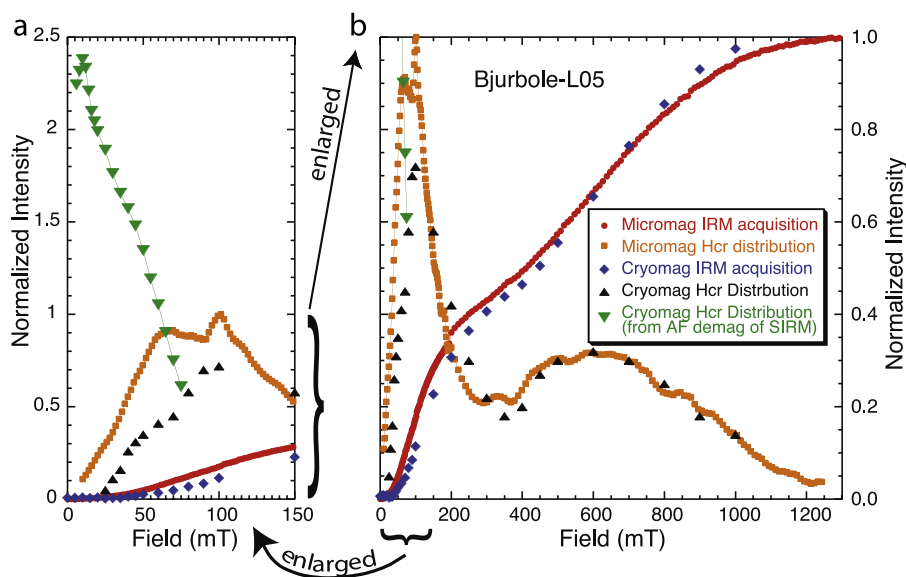
Figure 6. IRM acquisition and remanent coercivity distribution for a Bjurbole chondrule using different magnetometers and different methods for calculating the coercivity distribution. The MicroMag H_{cr} distribution (squares) and one of the Cryomag H_{cr} (triangles) distributions are obtained from derivates of the MicroMag and Cryomag IRM acquisitions curves, respectively. The other Cryomag H_{cr} distribution (inverted triangles) is obtained from derivatives of the AF demagnetization of the SIRM. (a) Large-amplitude low-coercivity component shown with the coercivity axis expanded to illustrate the width of the low-coercivity component. (b) Higher-coercivity components illustrated over the full field range (0–1300 mT).

presence of a magnetic field, both the induced magnetization and remanent magnetization contribute to the total coercivity spectrum.

[37] A standard FORC diagram has a coercivity axis (B_c or H_c) and a bias or interaction axis (B_b or H_b, also referred to as H_u in the nomenclature of *Pike et al.* [2001b]). In the absence of interactions, each distinct component of the coercivity distribution gives rise to a peak or ridge along the zero bias ($B_b = 0$) axis of a FORC diagram. Interactions between components can displace the coercivity components off the zero bias axis and/or can lead to the development of ridges that extend at angles of 45° from the zero bias axis. The ridges result from the switching of grains at applied fields slightly lower or higher than the true coercivity due to the influence of the magnetic fields of neighboring grains. For example, no grain can have a negative coercivity but a ridge trending 135° across a FORC diagram can be built by grains that switch before the polarity of the applied field actually changes sign.

[38] The FORC diagrams for the chondrules and bulk meteorites display three primary types of coercivity distributions, which we refer to as A, K, and B because the types of distributions correspond to the three sources of chondrules (Figures 9–11 and Table 1). Type-A FORC distributions are represented by the highest-coercivity Allende chondrules (Allende4284-CHA and Allende4327-CH1, -CH2, and -CH5). They have FORC distributions that extend out to about 250–350 mT, with little or no interaction above ~15 mT (Figure 10). These types of distributions are similar to those of basaltic glass where titanomagnetite grain sizes range from SP to small PSD and the grains are dispersed well enough that interactions are negligible. Not all Allende

chondrules have purely type-A FORC distributions. Some have distributions that have both A and K type affinities (Figure 10).

[39] Type-K FORC distributions, which are representative of all Karoonda chondrules, are triangular-shaped, indicating a continuum of interactions between grains of different coercivities (Figures 9 and 10). As noted above, the coercivity distributions are lognormal shaped, with a greater abundance of low-coercivity versus high-coercivity grains. This results in higher interactions at low coercivities with a progressive decay of interactions out to about 130 mT.

[40] Type-B FORC distributions, which are representative of all Bjurbole chondrules, are composed of several distinct coercivity components that are highly interactive. Most of the Bjurbole chondrules have a very large low-coercivity ridge with a smaller intermediate- (10 to 100 mT) coercivity lobe, which has a positive bias (i.e., plots in the upper half of the FORC diagram), and only a hint of an underlying very high coercivity component (Figures 9 and 10). The size of the low-coercivity ridge relative to the other components varies significantly enough that the other components can be masked completely (e.g., Bjurbole-02, Bjurbole-L07, and Bjurbole-L08). In a few chondrules, the intermediate- and high-coercivity components are comparable or larger than the low-coercivity ridge (e.g., in Bjurbole-L03, -L04, and -L05). Even when the low coercivity is large, the other components can generally be resolved by filtering out the ridge (Figure 10), which is done within program FORCIT. In cases where the high-coercivity component is well resolved, it has a Gaussian distribution that spans from about 200 to 900 mT with a peak between 400 to 700 mT (Figure 11).
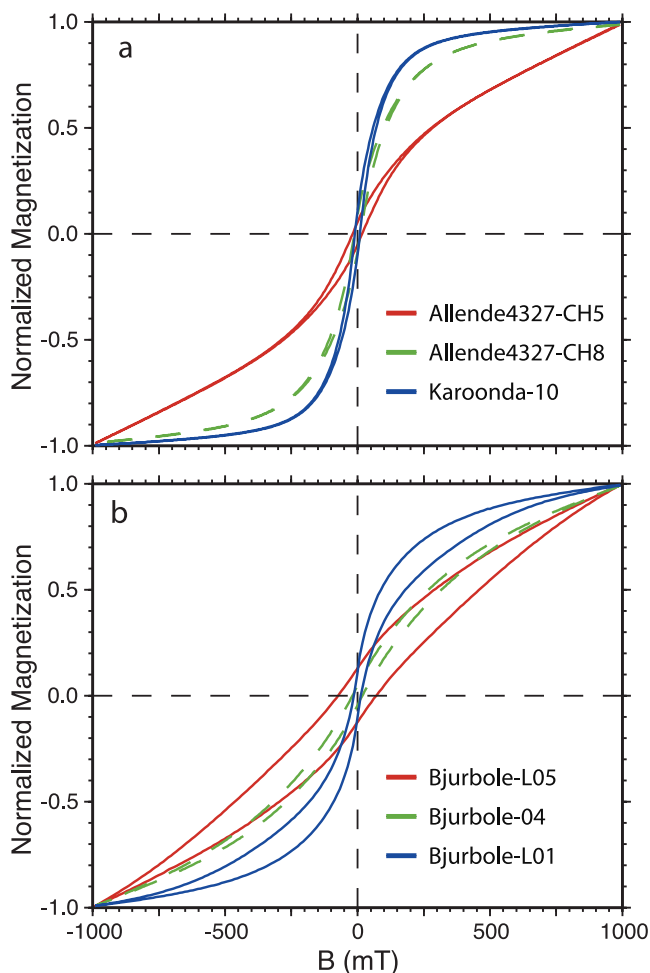
Figure 7. Representative hysteresis loops for (a) Allende, Karoonda, and (b) Bjurbole chondrules.

[41] For the Bjurbole chondrules, the interactions of the low- and the intermediate-coercivity distributions with each other and with the high-coercivity distribution produce one to three distinct ridges that start near the center of the low-coercivity distributions (i.e., near the origin of the FORC diagram or near the intermediate-coercivity component) and run at an angle of ~135° across the lower half of the diagram (Figure 11). The existence of switching prior to the change in the polarity of the field is revealed when the FORC distributions for the Bjurbole chondrules are mapped inside the hysteresis loop, which shows that much of the distribution occurs for negative applied fields (Figure 12). Similarly, the positive bias for the intermediate-coercivity distribution results from the grains with intermediate coercivity interacting with the magnetic fields from the neighboring grains with higher and lower coercivity. Both the bias and the 135° ridges are predicted by simple models of FORC distributions (Figure 13) [*Acton et al.*, 2005].

[42] Similar ridge-like features were observed in the micromagnetic models of *Carvallo et al.* [2003], where they were referred to as branches and attributed to interactions that occurred when the spacing between elongated particles became less than about two times the particle length. Also, *Chen et al.* [2005] observed ~135° ridges in their FORC diagrams, which resulted from an instrument artifact. We emphasize that the 135° ridges we observe for the Bjurbole chondrules emanate directly from individual coercivity distributions that are lower in coercivity than the highest-coercivity mode of the sample. The ridges are also much more pronounced than any source of instrument noise, can be reproduced on vibrating sample magnetometers and alternating gradient magnetometers, are observed in samples with two or more modes in their coercivity distributions, and are much more pronounced than in any other FORC diagram we have seen for terrestrial samples.
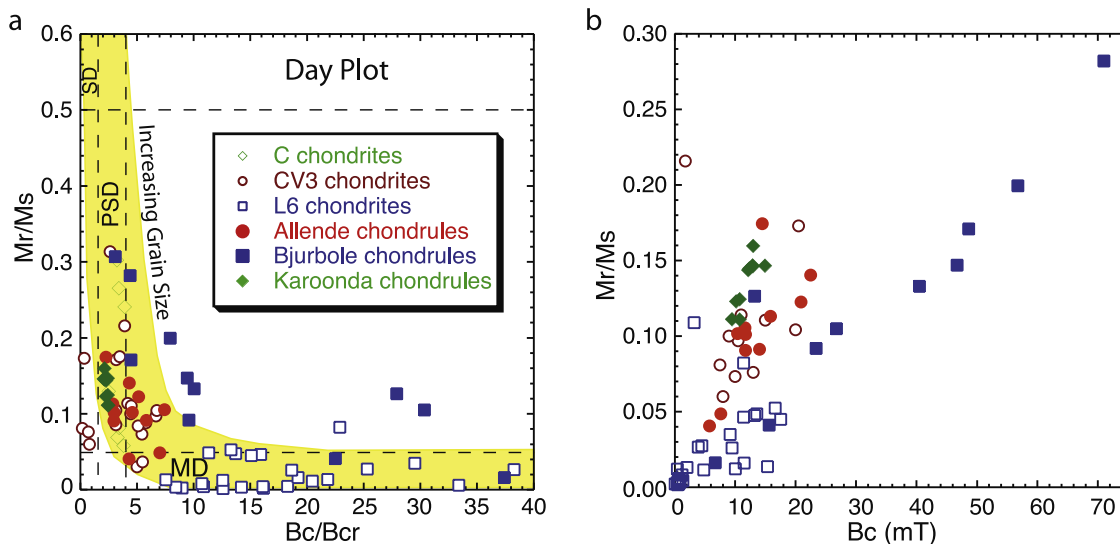

Figure 8. (a) Day plot for Allende (Al), Karoonda (Ka), and Bjurbole (Bj) chondrules along with results from several previous studies [*Nagata*, 1979; *Sugiura et al.*, 1979; *Funaki et al.*, 1981; *Wasilewski*, 1981a, 1981b; *Thorpe et al.*, 2002]. Note that the grain size fields (SD (single-domain), PSD (pseudosingle-domain), and MD (multidomain)) are those determined for magnetite and may not be directly indicative of the grain sizes for the magnetic minerals within the chondrules. (b) Variation of the coercivity of remanence (B_{cr}) versus M_r/M_s.
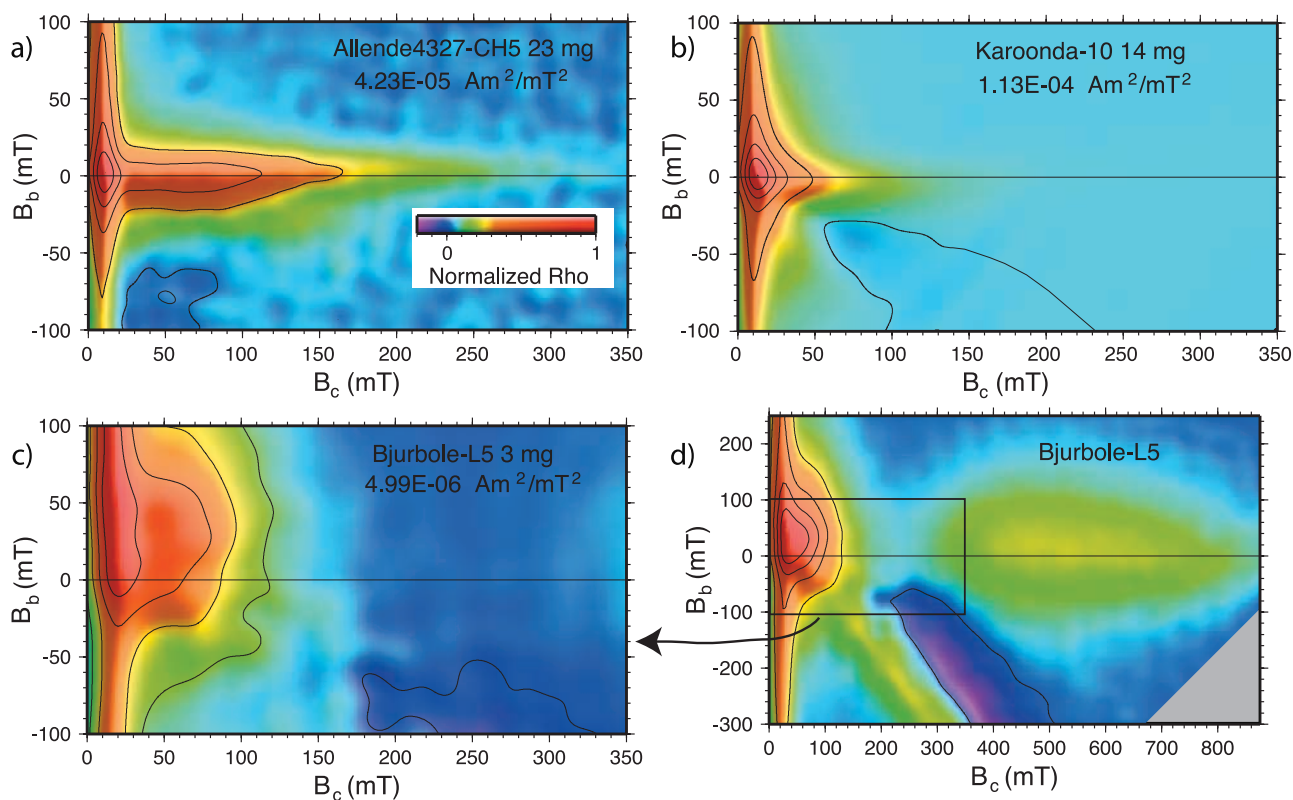
Figure 9. FORC diagrams illustrating the three primary types of coercivity distributions and magnetic interactions for chondrules examined in this study. The bias or interaction is B_b and the coercivity is B_c. (a) An Allende chondrule with A-type FORC distribution, (b) a Karoonda chondrule with K-type FORC distribution, (c) a Bjurbole chondrule with B-type FORC distribution, and (d) same as in Figure 9c except the view is expanded to illustrate the high-coercivity component and interactions.

4.7. Paleofield Estimates (REM, REMc, and REM′)

[43] The REM values in this study are comparable to those observed in past studies and are generally a factor of 2 to 10 larger than REMc values (Figure 14). The difference results from the existence of a significant low-coercivity component in most samples, which we interpret as due to secondary overprints. REMc values that include low AF demagnetization levels are influenced by low-coercivity overprints similar to the REM values (Figure 15). REMc values at high AF demagnetization levels can be influenced by noise (weak NRMs and spurious instrument-imparted ARMs). Our preferred REMc value is therefore the mean REMc value over the AF demagnetization interval that best defines the ChRM (Table 1). Within this interval, the REMc values are very stable as can be noted by the relatively small standard deviation, which averages 1×10^{-3} or about a third of the sample mean REMc value.

[44] REM′ values are very unstable for most demagnetization intervals over which the ChRM is resolved. The instability arises from the relatively high coercivity of the ChRM, which results in the intensity of the samples decaying little or none once the low-coercivity components have been removed by AF demagnetization. Derivatives of the change of NRM intensity with respect to the change in the AF demagnetization level are thus unstable, sometimes resulting in negative REM′ values. The fluctuations in the REM′ values are evident when computed between each AF demagnetization step within the AF demagnetization interval over which the ChRM is resolved. The standard deviation of these sample REM′ values is 1.6×10^{-2}, or more than an order of magnitude higher than the standard deviation of the REMc. Thus the REM′ method is not amenable to AF demagnetization results that give relatively stable endpoints on orthogonal vector diagrams.

[45] Our preferred paleofield estimator is the sample mean REMc value because it avoids the large biases caused by low-coercivity overprints that affect REM values and the instabilities caused by taking derivatives in the demagnetization data that affect the REM′ values. The weighted average of the sample mean REMc values are $3.48 \times 10^{-3} \pm 0.33 \times 10^{-3}$, $1.06 \times 10^{-3} \pm 0.06 \times 10^{-3}$, and $1.55 \times 10^{-3} \pm 0.35 \times 10^{-3}$ for Allende, Bjurbole, and Karoonda, respectively. If the REMc values are representative of the paleofield and, if the conversion factor of 3000 is accurate, then the paleofields recorded by the chondrules from Allende, Bjurbole, and Karoonda are 10.4 ± 1.0, 3.2 ± 0.2, and 4.6 ± 1.0 μT, respectively.

5. Discussion

5.1. Insights Into Chondrule Histories From Magnetic Properties

[46] Variations in the magnetic properties of the chondrules within and between meteorites provide evidence for different histories experienced by the chondrules before and
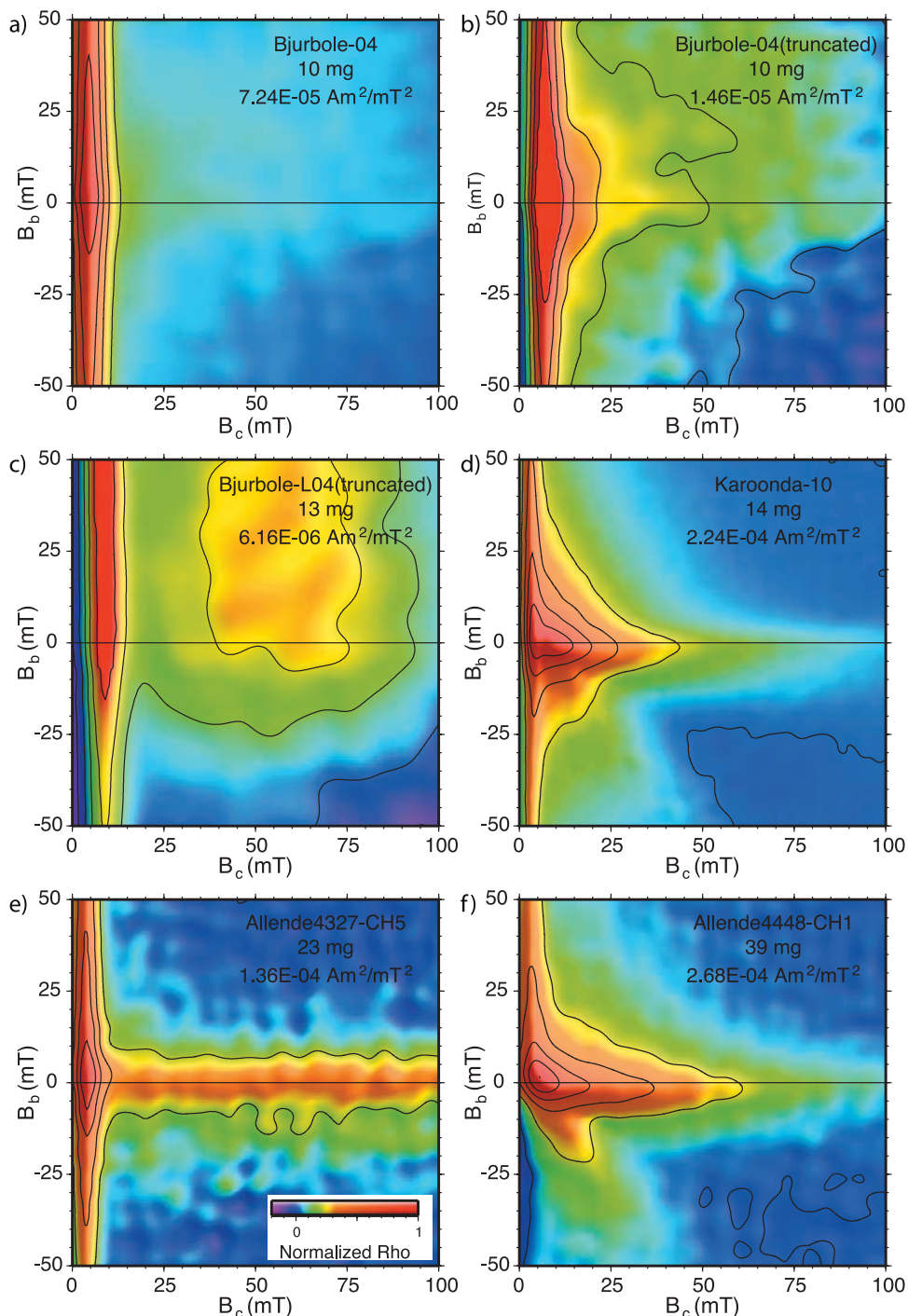
Figure 10. FORC diagrams that emphasis the coercivities <100 mT. (a) sample Bjurbole-04, (b) same as Figure 10a but with the low-coercivity ridge filtered and truncated to enhance the intermediate-coercivity component, (c) sample Bjurbole-L04 with the low-coercivity ridge filtered and truncated to enhance the intermediate-coercivity component, (d) sample Karoonda-10, (e) sample Allende4327-CH5, and (f) sample Allende4448-CH1. The bias or interaction is B_b, and the coercivity is B_c.

after accretion into a meteorite parent body. The variations within each meteorite are small relative to the variations between different meteorites.

[47] The within-meteorite magnetic properties indicate that the Karoonda chondrules are the most homogeneous. Each Karoonda chondrule has similar magnetic concentration, coercivity, interaction, and susceptibility. The grain size is also similar but there is a subtle correlation of increasing chondrule size with decreasing M_{rs}/M_s ratio, indicating the large chondrules have slightly larger magnetic grain sizes than small chondrules. We attribute this subtle difference in grain size to cooling rate variations, in which larger chondrules cool more slowly than smaller chondrules. Similar properties were noted in synthetic FeNi spheres
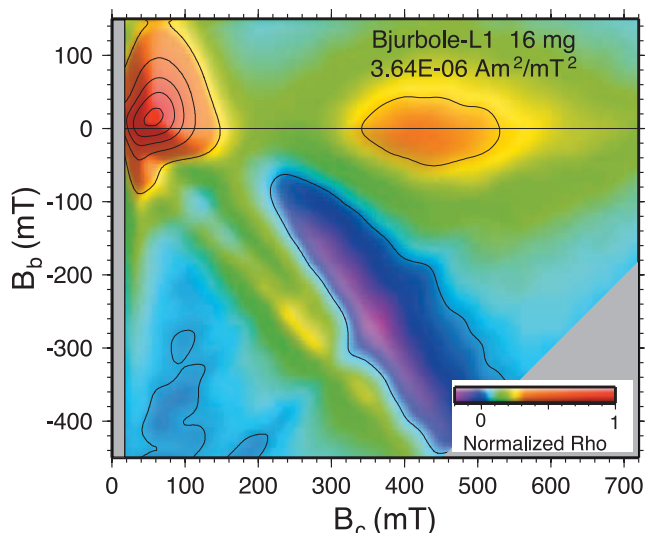
Figure 11. FORC diagram for chondrule Bjurbole-L01 with the low-coercivity ridge mostly filtered out (gray rectangle) to illustrate better the intermediate-coercivity component with its positive bias, the high-coercivity component, and the dual interaction ridges and the single interaction trough running at about 135° across the lower half of the diagram. The bias or interaction is B_b, and the coercivity is B_c.

studied by *Wasilewski* [1981b]. Overall, the Karoonda chondrules must have formed in a region with fairly homogeneous composition, cooled at only slightly different rates, and experienced similar conditions prior to and after amalgamation.

[48] The within-meteorite variations in the magnetic properties of Allende and Bjurbole chondrules are much greater than that observed for Karoonda chondrules. The within-meteorite variations of both susceptibility and saturation magnetization span more than 2 orders of magnitude, indicating significant differences in concentration of magnetic mineralogy. The differences in concentration lead to differences in magnetic interactions, where higher concentration results in higher interactions. Grain size and coercivity are also variable, with Bjurbole chondrules spanning more of the PSD and MD grain size region of the Day plot than both Karoonda and Allende chondrules combined. Interestingly, the largest Bjurbole chondrule (Bjurbole-L08, 75 mg) has the lowest susceptibility and saturation magnetization of all Bjurbole chondrules, a very large low-coercivity FORC distribution, and an extremely large B_{cr}/B_c ratio (~30). In contrast, the smallest Bjurbole chondrule (Bjurbole-L05, 3 mg) has no visible low-coercivity ridge in its FORC distribution and has the lowest B_{cr}/B_c ratio (~3). Again, we suggest these differences are mainly related to grain size, and to a lesser degree by grain shape, both of which may be partially limited by the physical size of the chondrule but is mainly controlled by cooling rate. No such relationship between grain size and chondrule size is evident in the Allende chondrules.
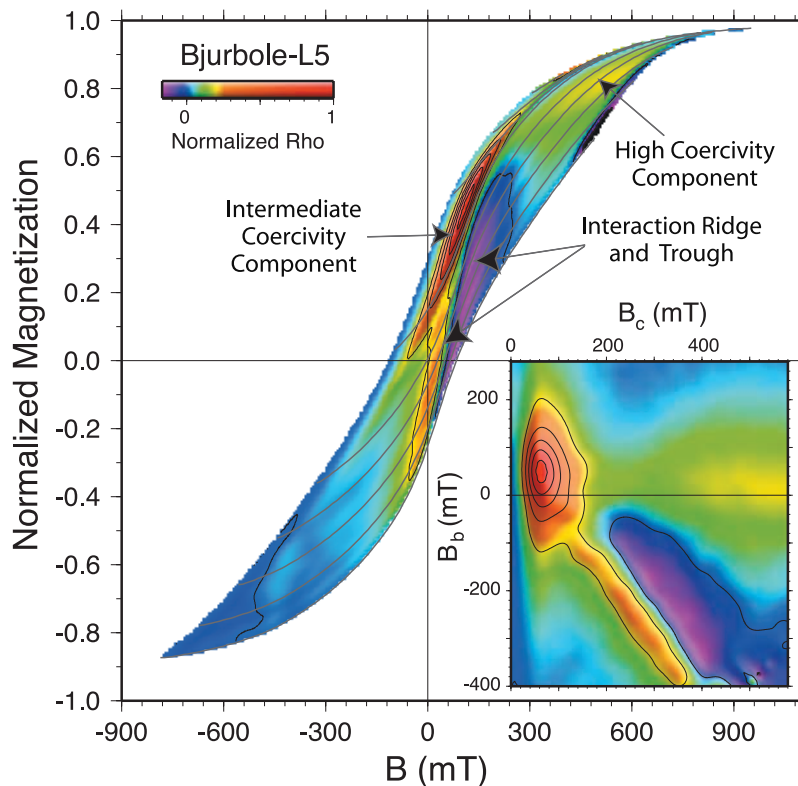

Figure 12. FORC distribution for chondrule Bjurbole-L05 plotted inside the hysteresis loop to illustrate where the interaction ridge and trough occur relative to the FORC paths (gray curves inside the hysteresis loop). Inset shows the associated FORC diagram. The bias or interaction is B_b, and the coercivity is B_c.

[49] Even though the Bjurbole chondrules display large grain size variations, they appear to have relatively homogenous magnetic mineral composition, in that all chondrules have a very high-coercivity component as is evident from the IRM demagnetization and acquisition data. Presumably this is tetrataenite as documented in Bjurbole chondrules by *Wasilewski* [1988]. The low- and intermediate-coercivity components may be larger-grained tetrataenite or, more likely, other magnetic minerals. Tetrataenite, which is commonly associated with taenite, forms below 350°C by slow cooling (0.1 to 100°C/m.y.) [*Clarke and Scott*, 1980]. The Bjurbole cooling rate has been estimated to be ~2°C/m.y. [*Willis and Goldstein*, 1981], which may have resulted from it cooling in the outer layers of a planetesimal [e.g., *Scott and Rajan*, 1981]. Apparently, the cooling rate for each chondrule varied significantly enough about the mean cooling rate to

permit the formation of different magnetic grain sizes. For variations in cooling rate to exist and for the Bjurbole chondrules to have NRM directions that are random with respect to each other within the Bjurbole meteorite, the chondrules may have had different locations within the planetesimal and must have been separated, perhaps by an impact with another body, before being accreted into the Bjurbole meteorite parent body.

[50] The absence of the very high coercivity component in Allende and Karoonda chondrules indicates an absence of tetrataenite. This is not surprising given that cooling rates for carbonaceous chondrites have been estimated to be 0.2°C/h up to 1000°C/h [*Lofgren*, 1996; *Meibom et al.*, 2000]. Differences in susceptibility, saturation magnetization, and coercivities between Allende and Karoonda indicate that they are derived from different source regions, with the source region for Allende being more heterogeneous or perhaps significantly larger than that for the Karoonda chondrules.

5.2. Coercivity Distributions, Interactions, and Paleointensities

[51] Convincing Thellier-Thellier paleointensity determinations on chondrules have not yet been obtained and doubt exists as to the validity of paleointensity estimates from REM, REMc, or REM′ values. Our study does not address whether any of the NRM/IRM ratios provide accurate paleointensity estimates, but it does provide insights into which chondrules have properties similar to natural materials that give reliable estimates as well as information about
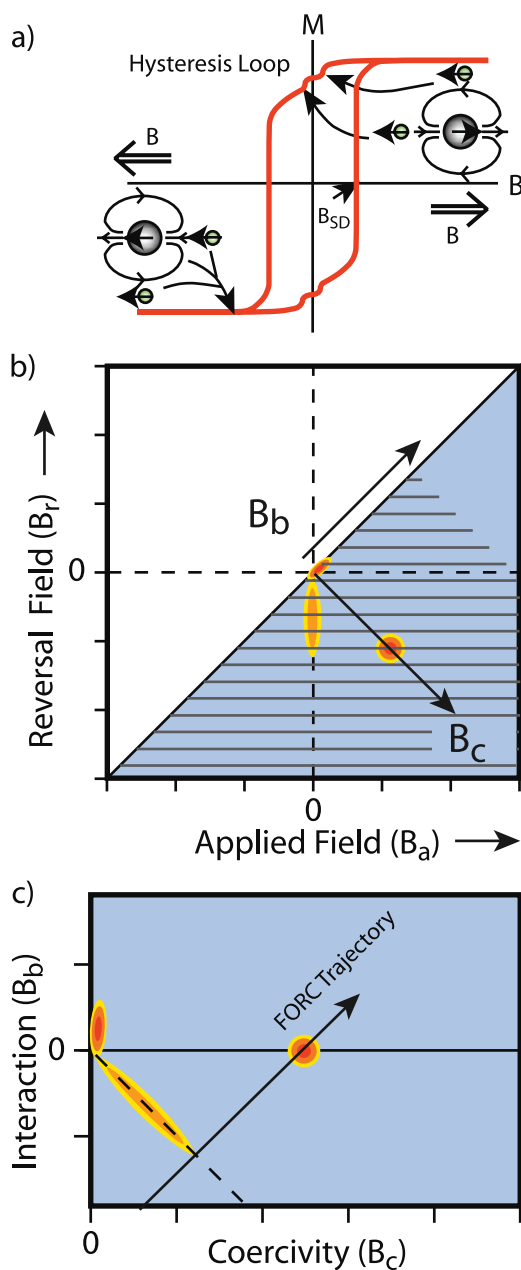

Figure 13. Schematic model illustrating how interactions between particles with different coercivities produce FORC distributions with positive bias (in this case, a positive low-coercivity ridge) and interaction ridges that trend ~135° across the lower portion of the FORC diagram. In the model, the small particles have very low coercivity (nearly super paramagnetic, SP) and interact with the larger single-domain (SD) particle, with coercivity B_{SD}. (a) Hysteresis loop shown with insets that illustrate the orientation of the moments for three magnetic grains for two instances along the hysteresis curve. For each inset, the applied field, B (i.e., the field of the electromagnet), is shown as an arrow with double lines. For a magnetic particle, the coercivity of the particle, the applied field, and the field of neighboring magnetic particles are what determine when the moment of the particle will flip or switch. (b) Resulting FORC distribution shown relative to the applied field (B_a) and reversal field (B_r) and (c) rotated into the standard orientation of FORC diagrams. The switching of the low-coercivity particles normally would only produce a FORC distribution at the true coercivity of the particles, which would be near zero B_b (the bias or interaction) and B_c (the coercivity) in this example. Owing to the interactions, which depend on the position of the low-coercivity particles relative to the high-coercivity particles, the low-coercivity component forms a low-coercivity ridge for positive B_b and a ridge that trends ~135° across the lower half of the FORC diagram. This 135° ridge forms near where the applied field changes sign.
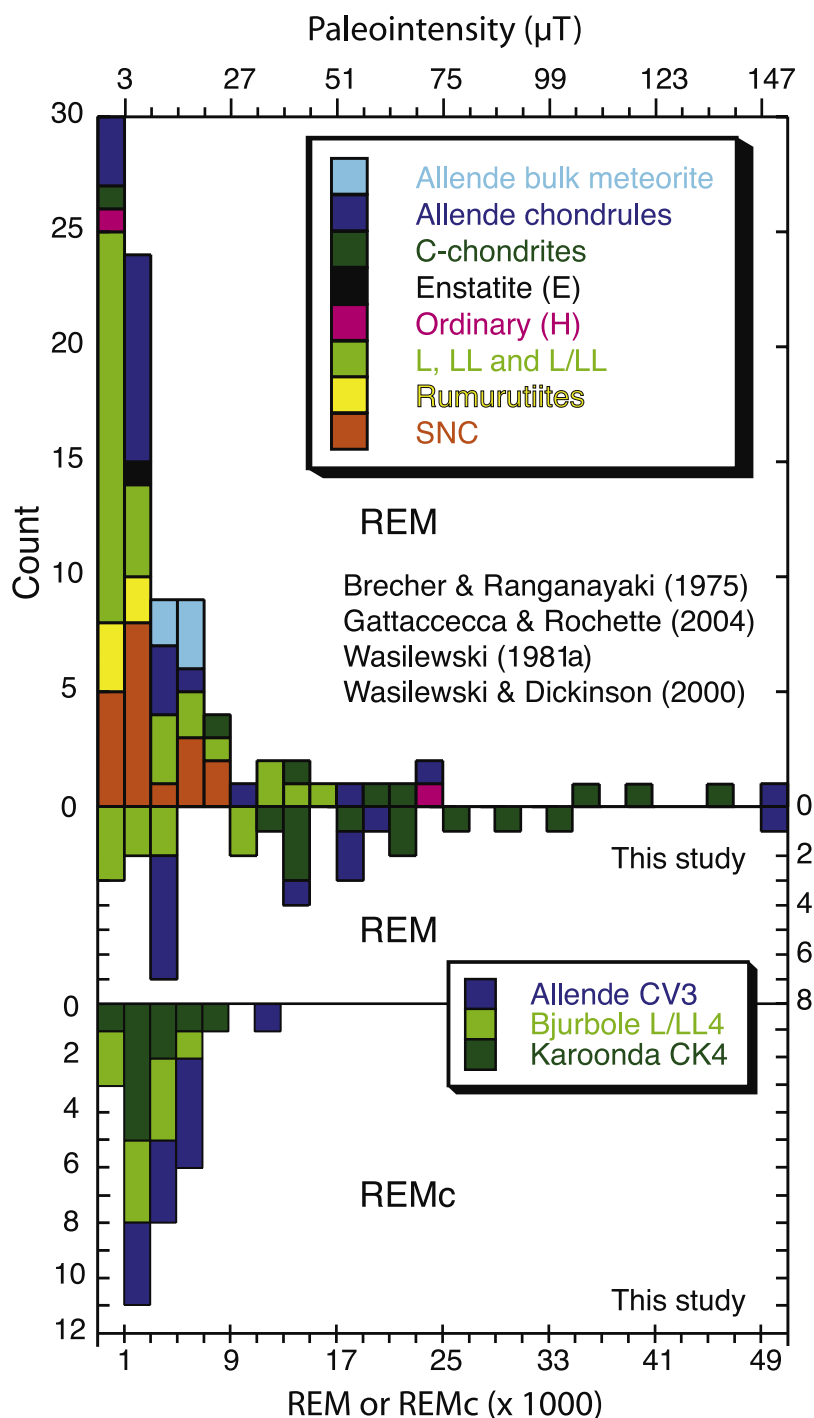
Figure 14. Histograms of REM values and estimated paleointensities from (top) previous studies [*Brecher and Ranganayaki*, 1975; *Wasilewski*, 1981a; *Wasilewski and Dickinson*, 2000; *Gattacceca and Rochette*, 2004] compared with (middle) REM and (bottom) REMc values from this study.

which NRM/IRM ratios are most likely to be biased by overprints or noise.

[52] Reliable paleointensity data are generally obtained from natural samples with SD or fine PSD grain sizes that have coercivity distributions extending well above 10 mT and that do not have large magnetic interactions [e.g., *Dunlop et al.*, 2005]. Basaltic glass and microcrystalline igneous rocks can have these attributes [e.g., *Selkin and Tauxe*, 2000]. The Allende chondrules have FORC distri-

butions most similar to fine-grained basalts and basaltic glass. The lower coercivity and larger magnetic interactions in the Karoonda chondrules are more typical of oceanic and ocean island basalts, which have higher failure rates in Thellier-Thellier paleointensity determinations although in some cases they can yield reliable determinations.

[53] The Bjurbole chondrules have FORC distributions quite unlike terrestrial rocks. The high-coercivity component is similar to hematite and the low-coercivity ridge is
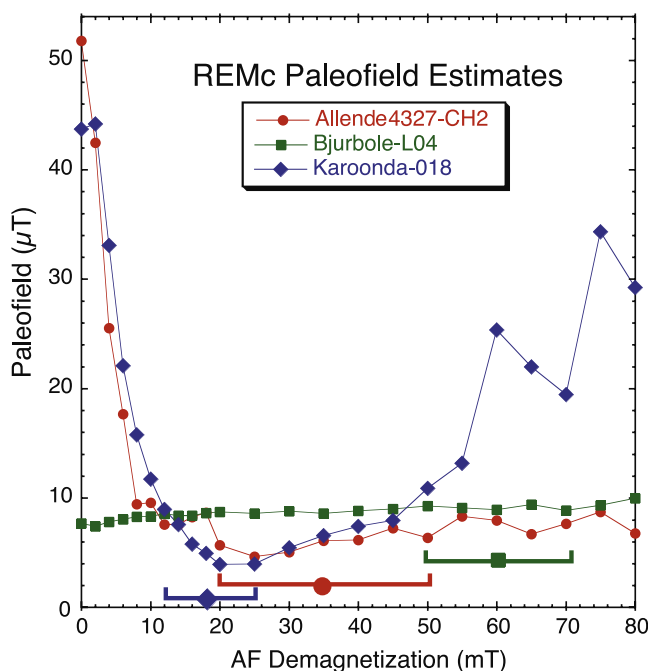
Figure 15. Variation of REMc (NRM/IRM ratio) with progressive AF demagnetization for representative (a) Allende, (b) Bjurbole, and (c) Karoonda chondrules.

similar to large multidomain magnetite, but the intermediate-coercivity lobe with positive bias and the strong interactions (the 135° ridges and trough) is not typical of other terrestrial rocks or synthetic mixtures we have produced using hematite, maghemite, magnetite, or goethite. Intuitively, such strong magnetic interactions have the potential to influence the ability of a rock to record accurately the strength of the paleofield.

[54] If NRM/IRM ratios can provide accurate paleointensity estimates, we suggest that the REMc values are most likely to provide unbiased estimates. The REM values can be strongly influenced by low-coercivity overprints. *Brecher and Ranganayaki* [1975] and *Gattacceca and Rochette* [2004] both make the point that using the NRM with no demagnetization results in an overestimate of the paleofield strength. Some degree of low-coercivity overprinting was apparent in most samples analyzed in this study. Paleointensities estimated from the resulting REM values were roughly an order of magnitude higher than those obtained from the REMc values, which depend on the more stably magnetized, higher-coercivity minerals. REM values were comparable to the REMc values (i.e., were within a factor of 2) for only 10 of 30 chondrules analyzed. Thus, while some chondrules may have escaped overprinting, most apparently have not.

[55] REM′ values are generally within a factor of 3 of the REMc values, with REM′ values being 40% higher on average. As noted in the results section, the REM′ values are much more variable when computed over the portion of the coercivity spectrum most representative of a stable ChRM.

[56] If the REMc values do give valid paleointensity estimates, then the Allende chondrules would more likely provide estimates of the intensity of magnetic fields of the early solar system as they are the only type 3 chondrite that we analyzed. In contrast, the Bjurbole chondrules are more likely to record the paleofield associated with or in the vicinity of the parent body in which the chondrules resided as they were heated and then slowly cooled, resulting in the formation of tetrataenite. Karoonda chondrules do not have the high-coercivity component related to formation of tetrataenite and so thermal alteration of these type 4 chondrites may not have been sufficient to reset the primary remanent magnetization. Even though Allende chondrules are the most pristine chondrules analyzed in this study, they may have sustained thermal alteration as suggested from petrographic analyses [*Brenker et al.*, 2002] and by Rb/Sr dating that indicate the age of the Allende chondrules was reset at 4.36 Ga [*Shimoda et al.*, 2005].

5.3. Magnetic Field of the Solar Nebula

[57] Assuming the Allende chondrules do record the paleointensity of the early solar system, which is quite speculative at this point, it is interesting to consider the implications. In the X wind model, chondrules are thought to have melted at a distance of 0.05 AU from the proto-Sun [*Shu et al.*, 1996]. Other models, such as the magnetorotational instability (MRI) model of *Joung et al.* [2004], predict that chondrules melt as far out as about 3 AU. Because the chondrules are heated and cooled rapidly, they would presumably record the paleofield in the vicinity of where they were heated.

[58] For Allende chondrules, that paleofield was apparently about 10 μT. For a dipole field with its axis aligned with the spin axis of the nebular disk, the dipole moment ($M = 4\pi Br^3/\mu_o$, where r = 0.05 to 3 AU, B = 1 $\times$ 10^{-5} T, μ_o = 4π $\times$ 10^{-7} H/m) in a vacuum would have been between 10^{30} to 10^{37} A m^2. The lower value is comparable to the dipole moment of the Sun ($\sim$5 $\times$ 10^{29} A m^2) [*Sakurai*, 1959]. Its worth noting, however, that the Sun's magnetic field observed at Earth is currently a few nannoteslas to a few tens of nannoteslas (e.g., http://www.spaceweather.com/) or about 2 to 3 orders of magnitude greater than that which would be created by the Sun's dipole field in a vacuum. The extra field is caused by heliospheric currents carried by the solar wind. Thus the current solar magnetic field at about 0.05 AU would be expected to be a couple orders of magnitude larger than that recorded by the chondrules but the current magnetic field may be a poor analogy to that of the early accretionary disk.

[59] Recent observations of the magnetic field of the protostellar accretion disk FU Orionis indicate that the magnitude of the radial field at 0.05 AU from the disk center is about 100 mT (1 kG), with an azimuthal field about half that value [*Donati et al.*, 2005]. These fields are about 4 orders of magnitude higher than the field recorded by Allende chondrules.

[60] It is tempting to conclude that the Allende chondrules were melted and cooled significantly further than 0.05 AU from the center of the disk. Many caveats exist to such a conclusion. First, it is not clear that any of the paleointensity proxies are accurate for fields higher than about 5 mT [see *Kletetschka et al.*, 2003, Figure 1]. The paleointensity recorded by the Allende chondrules is, however, well below this limit. Second, the paleofield recorded by Allende and other type 3 chondrites may have been reset

by thermal alteration [*Uehara and Nakamura*, 2006]. Third, even if the paleointensity signal was acquired immediately after chondrule formation, the chondrules were probably rotating rather than maintaining a constant position relative to the ambient magnetic field. According to three-dimensional structures of the chondrules obtained by X-ray microtomography [*Tsuchiyama et al.*, 2003], chondrules have experienced rapid spins of 50–350 rps or more during their formation. Unless the rotation axes of the chondrules were parallel to the magnetic field as they cooled rapidly to below the Curie temperature, the rotation would have the affect of partially demagnetizing the chondrules and the recorded paleointensity would be less than the true paleofield.

6. Conclusions

[61] Nondestructive measurements of magnetic properties provide a powerful method for discerning variations in the conditions under which different chondrules formed and for distinguishing between meteorites types. Magnetic properties of chondrules from the same meteorite vary much less than those of chondrules from different meteorites. Even so, the within-meteorite variations are sufficient to document changes in magnetic grain sizes that correlate with chondrule size as well as order of magnitude differences in magnetic concentration. The grain size variations could be caused by the larger chondrules cooling more slowly whereas the concentration variations may indicate heterogeneity in the source regions from which the chondrules were derived.

[62] Very distinct classes of FORC distributions exist for Allende, Karoonda, and Bjurbole chondrules. Coercivity distributions derived from the FORC diagrams and from IRM acquisition and demagnetization are Gamma distribution or lognormal shaped for Allende and Karoonda chondrules and are bimodal or trimodal for Bjurbole chondrules. The highest-coercivity mode in the Bjurbole chondrules is caused by tetrataenite, which interacts strongly with lower-coercivity components.

[63] Because a significant portion of the coercivity distributions for most chondrules is below 10 mT, low-coercivity magnetic overprints are common. Therefore paleointensities based on NRM/IRM ratios, without at least some magnetic cleaning, will probably be contaminated by overprinting. The resulting bias in the paleointensity estimate was found to be about an order of magnitude for many of the chondrules analyzed in this study.

[64] Paleointensity estimates based on NRM/IRM ratios following AF demagnetization (REMc values), although still unconfirmed by Thellier-Thellier determinations, indicate the paleofields recorded by the chondrules are roughly a third to a tenth of the geomagnetic field. Allende chondrules, which are the most pristine and possibly record the paleofield of the early solar system, have a weighted mean paleointensity of 10.4 ± 1.0 μT. Karoonda and Bjurbole chondrules, both of which have experienced some thermal alteration, were magnetized or possibly remagnetized in paleofields of 4.6 ± 1.0 and 3.2 ± 0.2 μT, respectively.

[65] Paleointensity study of FeNi alloys has a long way to go before NRM/IRM ratios should be directly translated into true paleofield estimates. Paleofields similar in intensity

to those quoted above have been noted to result from spontaneous remanence in iron meteorites [see *Dunlop and Özdemir*, 1997, section 17.4]. Furthermore, the strong magnetic interactions that occur within some of the chondrules may result in significant biases for any paleointensity method. In addition, low paleofields like those found in this study are near the lower limit to which the paleointensity proxies are applicable whereas fields generated near the centers of accretionary disks are near or above the upper limit of the proxies. Finally, the acquisition of magnetization by chondrules may be complicated by the rotation of chondrules as they cool through their Curie temperatures.

References

Acton, G., K. L. Verosub, A. Roth, and D. Linderholm (2005), Coercivity distributions and magnetic particle interactions from first-order reversal curves (FORCs): Examples from natural materials and software for data analysis, *Eos Trans. AGU*, 86(52), Fall Meeting Suppl., Abstract GP13A-0044.

Antretter, M., and M. Fuller (2002), Paleomagnetism and rock magnetism of Martian meteorite ALH 84001, *Phys. Chem. Earth, Parts ABC*, 27, 1299–1303.

Banerjee, S. K., and R. B. Hargraves (1972), Natural remanent magnetizations of carbonaceous chondrites and the magnetic field in the early solar system, *Earth Planet. Sci. Lett.*, 17, 110–119.

Brecher, A. (1977), Meteoritic magnetism: Implications for parent bodies of origin, in *Comets, Asteroid and Meteorites*, edited by A. H. Delsemme, pp. 415–427, Univ. Toledo Press, Toledo, Ohio.

Brecher, A., and G. Arrhenius (1974), The paleomagnetic record in carbonaceous chondrites: Natural remanence and magnetic properties, *J. Geophys. Res.*, 79, 2081–2106.

Brecher, A., and L. Leung (1979), Ancient magnetic field determinations on selected chondritic meteorites, *Phys. Earth Planet. Inter.*, 20, 361–378.

Brecher, A., and R. P. Ranganayaki (1975), Paleomagnetic systematics of ordinary chondrites, *Earth Planet. Sci. Lett.*, 25, 57–67.

Brenker, F. E., A. N. Krot, and P. H. Warren (2002), Evidence for a high temperature episode during multistage alteration of Allende dark inclusions, *Meteorit. Planet. Sci.*, 37, suppl., 24.

Butler, R. F. (1972), Natural remanent magnetization and thermomagnetic properties of the Allende meteorite, *Earth Planet. Sci. Lett.*, 17, 120–128.

Carvallo, C., A. R. Muxworthy, D. J. Dunlop, and W. Williams (2003), Micromagnetic modeling of first-order reversal curve (FORC) diagrams for single-domain and pseudo-single-domain magnetite, *Earth Planet. Sci. Lett.*, 213, 375–390.

Chen, A. P., R. Egli, and B. Moskowitz (2005), A FORC in the road?, *IRM Q.*, 15(3), 1–11.

Cisowski, S. M., and M. Fuller (1986), Lunar paleointensities via the IRMs normalization method and the early magnetic history of the Moon, in *Origin of the Moon: Proceedings of the Conference, Kona, HI, October 13–16, 1984*, edited by W. K. Hartmann, R. J. Phillips, and G. J. Taylor, pp. 411–424, Lunar and Planet. Inst., Houston, Tex.

Clarke, R. S., Jr., and E. R. D. Scott (1980), Tetrataenite; ordered FeNi, a new mineral in meteorites, *Am. Mineral.*, 65, 624–630.

Collinson, D. W. (1987), Magnetic properties of the Olivenza meteorite—Possible implications for its evolution and an early solar system, *Earth Planet. Sci. Lett.*, 84, 369–380.

Day, R., M. Fuller, and V. A. Schmidt (1977), Hysteresis properties of titanomagnetites: Grain-size and compositional dependence, *Phys. Earth Planet. Inter.*, 13, 260–267.

Donati, J.-F., F. Paletou, J. Bouvier, and J. Ferreira (2005), Direct detection of a magnetic field in the innermost regions of an accretion disk, *Nature*, 438, 466–469.

Dunlop, D. J. and Ö. Özdemir (1997), *Rock Magnetism: Fundamentals and Frontiers*, 573 pp., Cambridge Univ. Press, New York.

Dunlop, D. J., B. Zhang, and Ö. Özdemir (2005), Linear and nonlinear Thellier paleointensity behavior of natural minerals, *J. Geophys. Res.*, 110, B01103, doi:10.1029/2004JB003095.

Ebel, D. S., M. L. Rivers, and M. K. Weisberg (2007), Meteorite 3-dimensional synchrotron micro-tomography: Methods and applications, *Meteorit. Planet. Sci.*, in press.

Egli, R. (2004), Characterization of individual rock magnetic components by analysis of remanence curves: 2. Fundamental properties of coercivity distributions, *Phys. Chem. Earth, Parts ABC*, 29, 851–867.

Ferreira, J. (1997), Magnetically-driven jets from Keplerian accretion disks, *Astron. Astrophys.*, 319, 340–359.

Funaki, M., T. Nagata, and K. Momose (1981), Natural remanent magnetizations of chondrules, metallic grains and matrix of an Antarctic chondrite, ALH-769, *Mem. Nat. Inst. Polar Res. Spec. Issue*, 20, 300–315.

Gattacceca, J., and P. Rochette (2004), Toward a robust normalized magnetic paleointensity method applied to meteorites, *Earth Planet. Sci. Lett.*, 227, 377–393.

Herndon, J. M., M. W. Rowe, E. E. Larson, and D. E. Watson (1976), Thermomagnetic analysis of meteorites; 3, C3 and C4 chondrites, *Earth Planet. Sci. Lett.*, 29, 283–290.

Joung, M. K. R., M.-M. M. Low, and D. Ebel (2004), Chondrule formation and protoplanetary disk heating by current sheets in nonideal magneto-hydrodynamic turbulence, *Astrophys. J.*, 606, 532–541.

Kletetschka, G., T. Kohout, and P. Wasilewski (2003), Magnetic remanence in the Murchison meteorite, *Meteorit. Planet. Sci.*, 38, 399–405.

Kletetschka, G., M. H. Acuna, T. Kohout, P. J. Wasilewski, and J. E. P. Connerney (2004), An empirical scaling law for acquisition of thermoremanent magnetization, *Earth Planet. Sci. Lett.*, 226, 521–528.

Kletetschka, G., T. Kohout, P. J. Wasilewski, and M. Fuller (2005), Recognition of thermal remanent magnetization in rocks and meteorites, paper presented at 10th Scientific Assembly of the International Association of Geomagnetism and Aeronomy, Toulouse, France.

Kletetschka, G., M. D. Fuller, T. Kohout, P. J. Wasilewski, E. Herrero-Bervera, N. F. Ness, and M. H. Acuna (2006), TRM in low magnetic fields: A minimum field that can be recorded by large multidomain grains, *Phys. Earth Planet. Inter.*, 154, 290–298.

Kohout, T., G. Kletetschka, M. Kobr, P. Pruner, and P. J. Wasilewski (2004), The influence of terrestrial processes on meteorite magnetic records, *Phys. Chem. Earth, Parts ABC*, 29, 885–897.

Lanoix, M., and D. W. Strangway (1978), The magnetic remanence carried by Allende chondrules, *Meteoritics*, 13, 531–536.

Lanoix, M., D. W. Strangway, and G. W. Pearce (1977), Anomalous acquisition of thermoremanence at 130C in iron and paleointensity of the Allende meteorite, *Proc. Lunar Sci. Conf.*, 8, 689–701.

Lofgren, G. E. (1996), A dynamic crystallization model for chondrule melts, in *Chondrules and the Protoplanetary Disk*, edited by R. H. Hewins, R. H. Jones and E. R. D. Scott, pp. 187–196, Cambridge Univ. Press, New York.

Meibom, A., S. J. Desch, A. N. Krot, J. N. Cuzzi, M. I. Petaev, L. Wilson, and K. Keil (2000), Large-scale thermal events in the solar nebula; evidence from Fe, Ni metal grains in primitive meteorites, *Science*, 288, 839–841.

Morden, S. J. (1992), The anomalous demagnetization behaviour of chondritic meteorites, *Phys. Earth Planet. Inter.*, 71, 189–204.

Morden, S. J., and D. W. Collinson (1992), The implications of the magnetism of ordinary chondrite meteorites, *Earth Planet. Sci. Lett.*, 109, 185–205.

Muxworthy, A. R., and D. J. Dunlop (2002), First-order reversal curve (FORC) diagrams for pseudo-single-domain magnetites at high temperature, *Earth Planet. Sci. Lett.*, 203, 369–382.

Nagata, T. (1979), Meteorite magnetism and the early solar system magnetic field, *Phys. Earth Planet. Inter.*, 20, 324–341.

Pike, C. R., A. P. Roberts, and K. L. Verosub (1999), Characterizing interactions in fine magnetic particle systems using first order reversal curves, *J. Appl. Phys.*, 85, 6660–6667.

Pike, C. R., A. P. Roberts, M. J. Dekkers, and K. L. Verosub (2001a), An investigation of multi-domain hysteresis mechanisms using FORC diagrams, *Phys. Earth Planet. Inter.*, 126, 11–25.

Pike, C. R., A. P. Roberts, and K. L. Verosub (2001b), First-order reversal curve diagrams and thermal relaxation effects in magnetic particles, *Geophys. J. Int.*, 145, 721–730.

Roberts, A. P., C. R. Pike, and K. L. Verosub (2000), First-order reversal curve diagrams: A new tool for characterizing the magnetic properties of natural samples, *J. Geophys. Res.*, 105, 28,461–28,475.

Rochette, P., L. Sagnotti, M. Bourot-Denise, G. Consolmagno, L. Folco, J. Gattacceca, M. L. Osete, and L. Pesonen (2003), Magnetic classification of stony meteorites; 1, Ordinary chondrites, *Meteorit. Planet. Sci.*, 38, 251–268.

Sakurai, L. (1959), Motions of solar cosmic rays and the properties of the general magnetic field of the Sun, *J. Geomagn. Geoelectr.*, 11, 21–33.

Scott, E. R. D., and R. S. Rajan (1981), Polycrystalline taenite and metallographic cooling rates of chondrites; reply to comments of A. W. R. Bevan and H. J. Axon, *Geochim. Cosmochim. Acta*, 45, 1959.

Selkin, P. A., and L. Tauxe (2000), Long-term variations in palaeointensity, *Phil. Trans. R. Soc. London, Ser. A*, 358, 1065–1088.

Shimoda, G., N. Nakamura, M. Kimura, T. Kani, S. Nohda, and K. Yamamoto (2005), Evidence from the Rb-Sr system for 4.4 Ga alteration of chondrules in the Allende (CV3) parent body, *Meteorit. Planet. Sci.*, 40, 1059–1072.

Shive, P. J. (1986), Suggestions for the use of SI units in magnetism, *Eos Trans. AGU*, 67, 25.

Shu, F. H., H. Shang, and T. Lee (1996), Toward an astrophysical theory of chondrites, *Science*, 271, 1545–1552.

Shu, F. H., H. Shang, A. E. Glassgold, and T. Lee (1997), X-rays and fluctuating X-winds from protostars, *Science*, 277, 1475–1479.

Stacey, F. D. (1976), Paleomagnetism of meteorites, *Annu. Rev. Earth Planet. Sci.*, 4, 147–157.

Sugiura, N., and D. W. Strangway (1985), NRM directions around a centimeter-sized dark inclusion in Allende, *Proc. Lunar Planet. Sci. Conf., 15th, J. Geophys. Res.*, 90, C729–C738.

Sugiura, N., and D. W. Strangway (1988), Magnetic studies of meteorites, in *Meteorites and the Early Solar System*, edited by J. F. Kerridge and M. S. Matthews, pp. 595–615, Univ. of Ariz. Press, Tucson.

Sugiura, N., M. Lanoix, and D. W. Strangway (1979), Magnetic fields of the solar nebula as recorded in chondrules from the Allende meteorite, *Phys. Earth Planet. Inter.*, 20, 342–349.

Thorpe, A. N., F. E. Senftle, and J. R. Grant (2002), Magnetic study of magnetite in the Tagish Lack meteorite, *Meteorit. Planet. Sci.*, 37, 763–771.

Tsuchiyama, A., R. Shigeyoshi, T. Kawabata, T. Nakano, K. Uesugi, and S. Shirono (2003), Three-dimensional structures of chondrules and their high-speed rotation, *Annu. Lunar Planet. Sci. Conf., 34th*, Abstract A1271.

Uehara, M., and N. Nakamura (2006), Experimental constraints on magnetic stability of chondrules and the paleomagnetic significance of dusty olivines, *Earth Planet. Sci. Lett.*, 250, 292–305.

Valet, J. (2003), Time variations in geomagnetic intensity, *Rev. Geophys.*, 41(1), 1004, doi:10.1029/2001RG000104.

Wasilewski, P. J. (1973), Magnetic hysteresis in natural materials, *Earth Planet. Sci. Lett.*, 20, 67–72.

Wasilewski, P. (1981a), New magnetic results from Allende C3(V), *Phys. Earth Planet. Inter.*, 26, 134–148.

Wasilewski, P. (1981b), Magnetization of small iron-nickel spheres, *Phys. Earth Planet. Inter.*, 26, 149–161.

Wasilewski, P. (1988), Magnetic characterization of the new magnetic mineral tetrataenite and its contrast with isochemical taenite, *Phys. Earth Planet. Inter.*, 52, 150–158.

Wasilewski, P. J., and T. Dickinson (2000), Aspects of the validation of magnetic remanence in meteorites, *Meteorit. Planet. Sci.*, 35, 537–544.

Wasilewski, P., M. H. Acuna, and G. Kletetschka (2002), 433 Eros: Problems with the meteorite magmatism record in attempting an asteroid match, *Meteorit. Planet. Sci.*, 37, 937–950.

Willis, J., and J. I. Goldstein (1981), A revision of metallographic cooling rate curves for chondrites, *Proc. Lunar Planet. Sci. Conf.*, 12, Part B, 1135–1143.

Yu, Y. (2006), How accurately can the NRM/SIRM determine the ancient planetary magnetic field intensity?, *Earth Planet. Sci. Lett.*, 250, 27–37.

———————————

G. Acton, B. Jacobsen, A. Roth, K. L. Verosub, and Q.-Z. Yin, Department of Geology, University of California, One Shields Avenue, Davis, CA 95615, USA. (acton@geology.ucdavis.edu)

D. S. Ebel, Department of Earth and Planetary Sciences, American Museum of Natural History, New York, NY 10024, USA.

L. Jovane, Istituto Nazionale di Geofisica e Vulcanologia, Via di Vigna Murata, I-60500143 Rome, Italy.